



UIT

NORGES
ARKTISKE
UNIVERSITET

Faculty of Science and Technology

Department of Geosciences

Reconstruction of the bottom current strength of overflow water through the Faeroe-Shetland Channel in relation to climate change during the last 135,000 years

—

Martin Solheim

Master thesis in Geology [GEO-3900]

May 2018



Abstract

The focus of this thesis was to reconstruct the bottom current strength around the Faeroe Islands and relate it to the climate variability over the past 35,000 - 135,000 years and the Holocene, using the piston core, JM11-FI-19PC, taken on the Fugløy Ridge, from the North-eastern shelf of the Faeroe Islands. The core location is ideal for measuring the overflow from the Nordic Seas, as it is strategically placed on top of the Greenland-Scotland Ridge, where cold bottom water from the Greenland Sea passes over the core, before entering the North Atlantic Ocean through the Faeroe-Shetland Channel.

The investigated time interval includes the last glacial cycle, Weichselian, as well as the two interglacials, the Holocene and Eemian. The results are based on sortable silt analysis, IRD and tephra counts, as well as material from previous studies of the investigated core.

The results from this thesis is linking higher bottom current strength with interstadials throughout the Weichselian ice age, but also demonstrating that the circulation around the Faeroe Islands never ceased, but reversed. Material from other sources have provided evidence for a warm, subsurface current entering the Nordic Seas during stadials, and the results from this thesis demonstrate that there was a weaker current flowing over the investigated core during stadials.

The bottom current strength measured in the results show clear relations to the climatic variabilities throughout the last glacial cycle, and also strongly suggest vertical shifts of currents and water masses, that are likely to be connected to the relative sea level.

The length of the core also presents the opportunity to compare the two interglacials; the Holocene and the Eemian. Similarities within these interglacials have been found, and there are indications that the Eemian might serve as a precursor for the present-day conditions of the climate.

Acknowledgements

I would like to give a big thanks to my supervisor Tine L. Rasmussen for providing great support when I had anything I was uncertain about. Thanks to my co-supervisors, Juho Junttila for all the help with the sortable silt and lab work, and a huge thanks to Mohamed M. Ezat for providing all the extra material I needed for the thesis!

I would also like to thank the laboratory staff Trine Dahl, Ingvild Hald and Karina Monsen for all the help they provided me with during my laboratory work.

Thank you to all my fellow master students, for being such a welcoming bunch of people, making the transition from Bergen to Tromsø so fantastic!

A big thank to my friends who joined me from UiB, Asbjørn Hetland and Lars T. Christiansen, for making it so easy to find roommates in Tromsø when we first moved here, for all the good and stupid conversations and for keeping me sane through this last part before submitting!

Thanks to my family and especially to my parents, Aud Ingrid Espeland and Sigbjørn Solheim, for supporting me through all these years!

There is probably a bunch more I'm forgetting, but the credits are rolling!

Thank you, Tromsø!

Martin Solheim

Tromsø, 15.05.2018

Table of Contents

1. Introduction	1
1.1 Objectives.....	1
1.2 Study area	1
1.2.1 Location of the core	1
1.2.2 Oceanographical setting	2
1.3 Marine Isotope Stages (MIS)	5
1.4 History of ice core drilling in Greenland	6
1.5 Dansgaard/Oeschger Events	7
1.6 Heinrich Events.....	8
1.7 Proxies in marine cores.....	9
1.7.1 Sortable Silt as a proxy	9
1.7.2 Ice-Rafted Debris (IRD) as proxy.....	11
1.7.3 Tephra as proxy	11
1.7.4 Foraminifera as proxy	11
1.7.5 Magnetic Susceptibility as proxy	12
2 Methods and Materials	13
2.1 Materials from other sources	13
2.1.1 Multi-sensor Core Logger	14
2.1.2 Foraminifera assemblage.....	14
2.1.3 North Greenland Ice-core Project Oxygen Isotope Data.....	14
2.2 Sediment Coring	15
2.3 Sortable Silt	15
2.4. Ice-Rafted Detritus (IRD)	17
2.5. Tephra.....	18
3. Results	19
3.1 Results used from other sources.....	19
3.2 Sortable Silt	19
3.2.1 Unit 1 (375-695 cm).....	20
3.2.2 Unit 2 (675-930 cm).....	20
3.2.3 Unit 3 (905 – 1105 cm)	21
3.2.4 Unit 4 (5-85 cm).....	21
3.3 IRD – Ice Rafted Detritus.....	24
3.2.1 Unit 1 (375-695 cm).....	24

3.2.2	Unit 2 (675-930 cm).....	24
3.2.3	Unit 3 (905-1105 cm)	24
3.2.4	Unit 4; Holocene (5-85 cm)	25
3.4	Tephra	25
3.3.1	Unit 1 (375-695 cm).....	26
3.3.2	Unit 2 (675-930 cm).....	26
3.3.3	Unit 3 (905-1105 cm)	26
3.3.4	Unit 4; Holocene (5-85 cm)	27
3.5	Sand Calibration	27
3.6	Velocity estimates	32
3.7	Construction of the age model	33
4.	Discussion	37
4.1	Interpretation and age correlation.....	37
4.1.1	Unit 1: 375-695 cm	37
4.1.2	Unit 2: 675-930 cm	38
4.1.3	Unit 3: 905-1105 cm.....	40
4.1.4	Holocen: 5-85 cm	41
4.2	Comparison to other studies.....	44
4.3	Deep-water changes	48
4.3.1	Ice-rafted Silt Biasing.....	48
4.3.2	Bottom water current flow during stadials and interstadial.....	48
4.3.3	Convection and deep-water changes.....	52
4.3.4	Relative Sea Level.....	53
4.3.5	Marine Isotope Stages 3-4.....	57
4.4	The Holocene and the Eemian interglacials.....	59
5.	Conclusion	65
6.	References	67

1. Introduction

1.1 Objectives

The aim of this thesis is to reconstruct the bottom current strength of the overflow water passing through the Faeroe-Shetland Channel, as a measurement of the strength of the convection in the Nordic Seas. This will be related to climate variability during the past ~35,000-135,000 years, from the end of the Saale ice age to MIS 3, covering the Eemian and Holocene interglacials and the Weichselian ice age.

1.2 Study area

1.2.1 Location of the core

A deep-sea piston core (JM11-FI-19PC) had been retrieved from the northeastern shelf off the Faeroe Islands (Figure 1). The core location is situated about 120 km northeast off the Eastern coast of the Faeroe Islands (62°49'N, 03°52'W), on a ridge formation called the Fugløy Ridge. The *R/V Jan Mayen* took the core during a cruise for the University of Tromsø, on May 2, 2011 (Ezat, et al., 2014). The core was taken at water depth of 1179 m and penetrated 13 meters into the sediments. The core was split into 11 sections, containing 11.24 meters (see Table 1 in Chapter 2). The upper 10 cm was disturbed by “slushing” (From cruise data, provided by T. L. Rasmussen).

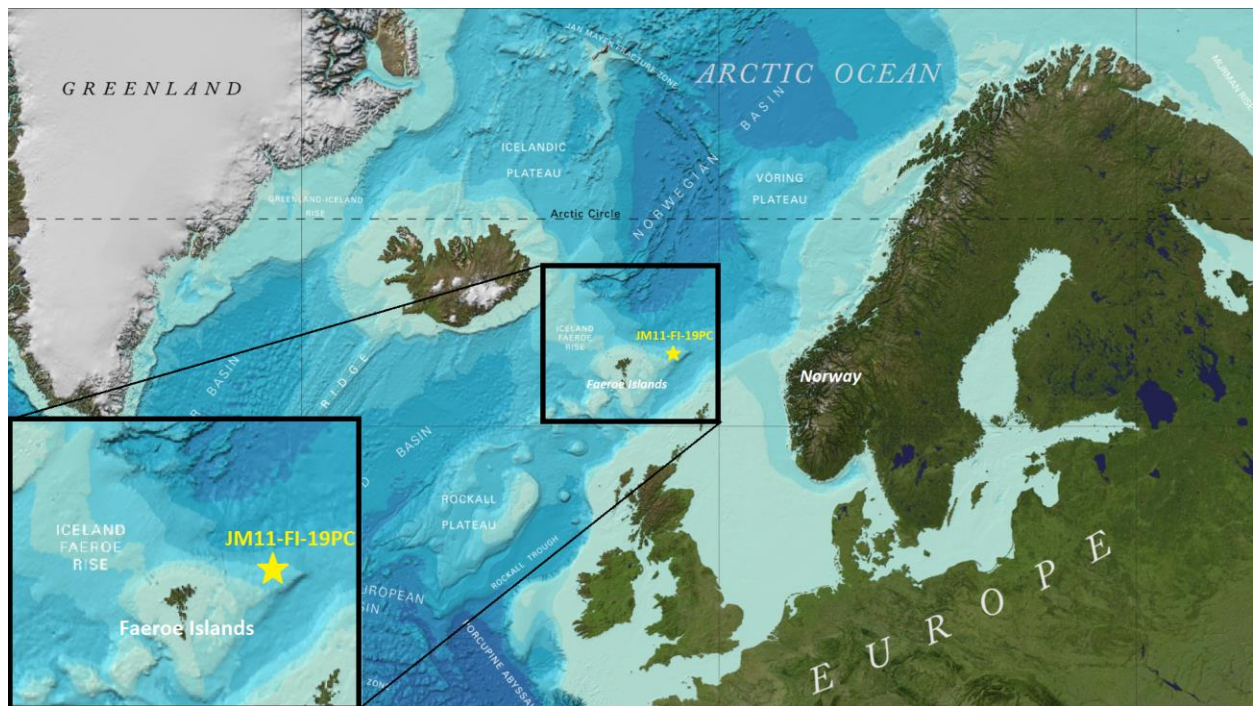


Figure 1: Overview photo of the North Atlantic (up to 72° N), with the investigated core, JM11-FI-19PC, marked with a yellow star. (Image reproduced from the GEBCO world map 2014, www.gebco.net)

1.2.2 Oceanographical setting

The Faeroe Islands lie on top of the Greenland-Scotland Ridge, placing it right in the middle of the North Atlantic Current (NAC) system. About one-third of the cold overflow from the Nordic Seas that crosses the Greenland-Scotland Ridge passes over the core location, as it flows underneath the warm Atlantic surface water (Ezat, et al., 2014). The North Atlantic stretches all the way up to the Arctic Ocean, transporting warm and saline Atlantic water northward along the Norwegian slope. As these waters travel northwards, as the North Atlantic Drift, they get cooled down and transfers heat to the atmosphere, giving northwestern Europe a warmer climate than corresponding latitudes elsewhere. (Figure 2).

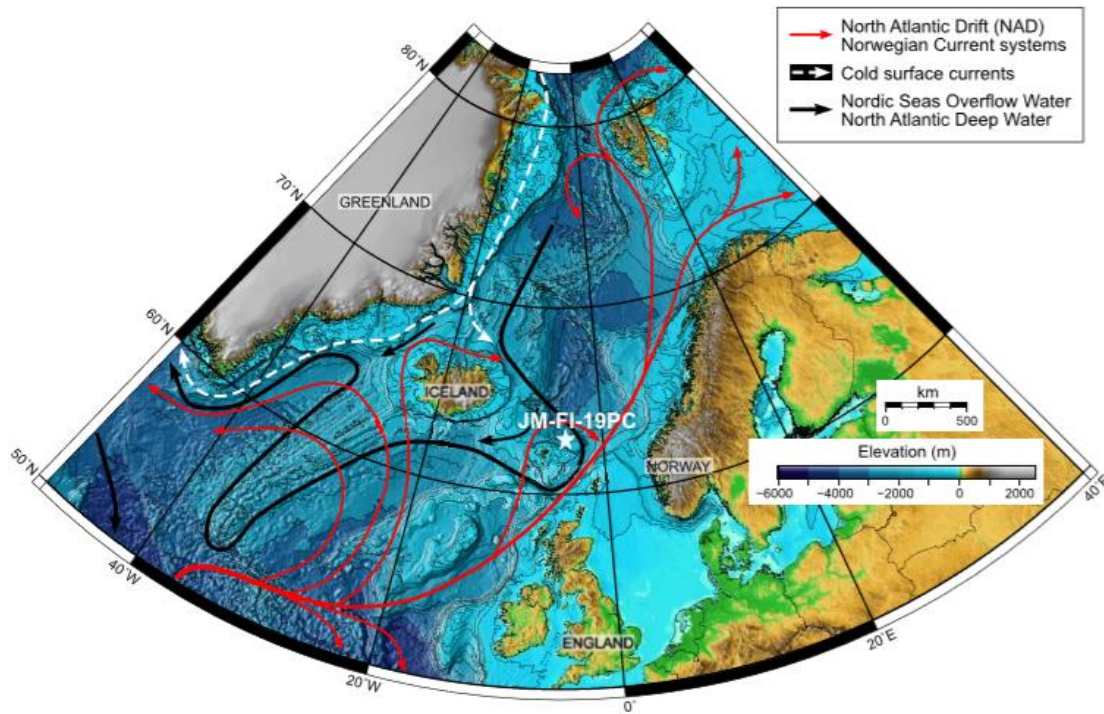


Figure 2: Core location with the North Atlantic Drift (red) and the Nordic Seas Overflow Water (black). Image modified from Ezat, et al. (2016)

As the warm waters gets cooler, the upper layers becomes denser and sinks deeper into the water column (Meincke, et al., 1997).

The Atlantic water flows northward along Norway as the Norwegian Atlantic Current, before it splits into two different parts. One travels further north over the Barents Sea, while the other branches into the West Spitsbergen Current entering through the Fram Strait. These warm waters flow through the Arctic Ocean, gets cooled down, before all loops join in the East Greenland Current (Rudels, et al., 2012).

Through this cooling process, the currents are divided into different density layers, depending on temperature and salinity. The densest of these layers are producing the North Atlantic Deep Water (NADW), which spills over the Greenland-Scotland Ridge at two major gateways; The Denmark Strait and the Faeroe-Shetland Channel (Kuijpers, et al., 1998). The Greenland Sea Deep Water (GSDW) passes through the Denmark Strait, while the Norwegian Sea Overflow Water (NSOW) passes through the Faeroe-Shetland channel. (Figure 3)

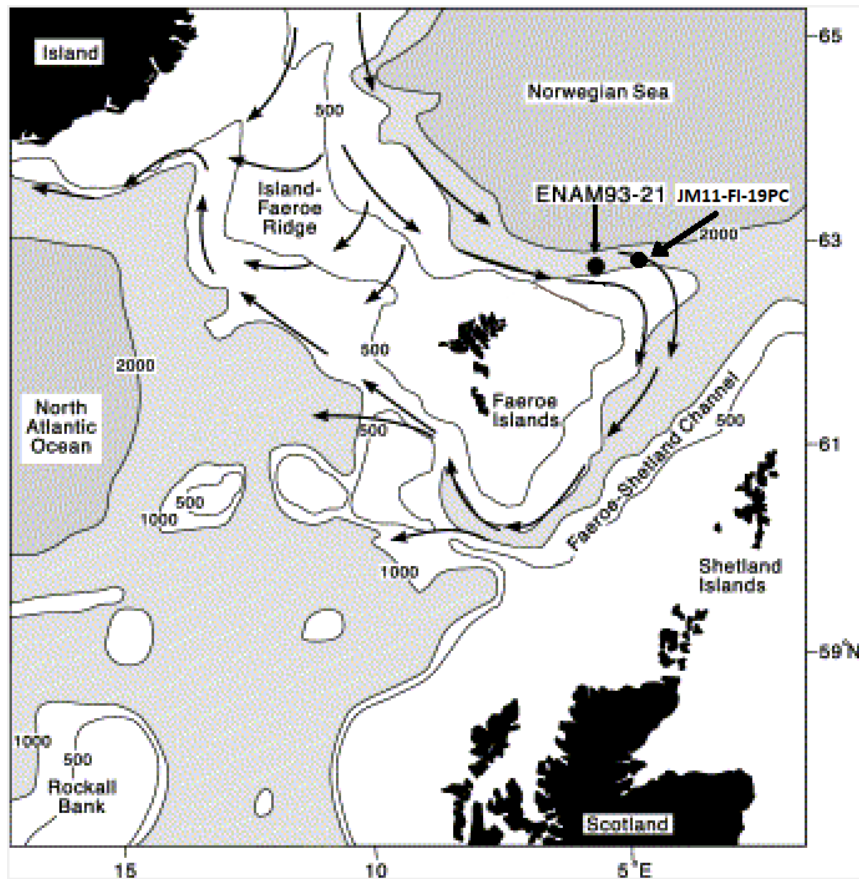


Figure 3: Image showing how the major subsurface, deep-waters are flowing past the Faeroe Islands and the core location. JM11-FI-19PC marked, as well as ENAM93-21, as it will be mentioned further down in the thesis. Image modified from Rasmussen, et al. (2003).

This system of ocean currents in the North Atlantic is called the Atlantic Meridional Overturning Circulation (AMOC), and it has a major impact on the climate. During the Quaternary Period, changes in the AMOC led to some of the strongest and fastest climate shifts (Caesar, et al., 2018). Long-term variations in the AMOC would be associated with big climatic changes, like the Dansgaard-Oeschger events (see below), notable in the ice cores from Greenland. Recent studies have however, shown that changes in the AMOC happens on centurial timescales as well (e.g. Thornalley, et al., (2018); Caesar, et al., (2018); Rudels, et al. (2012)). Since the layering of the AMOC is dependent on modest differences in density and salinity it seems that centurial changes, or even decadal- and annual changes, can affect it. Most of these changes are indirectly attributed to rising global temperatures. Caesar, et al. (2018), argues that the rise in temperature would increase the sea surface temperatures (SST), something that would decrease the density. Thornalley, et al. (2018), theorizes that

the weakening of the AMOC is due to freshwater input, reducing the salinity of the waters and inhibits the convection in the Labrador Sea.

Thermohaline differences was noted by Rudels, et al. (2012), on a decadal scale. He found differences in temperature and salinity in the layers of the Greenland Sea in the time span between 1998-2010, and showed how this would affect the water column in the Greenland and Norwegian Seas (Figure 4).

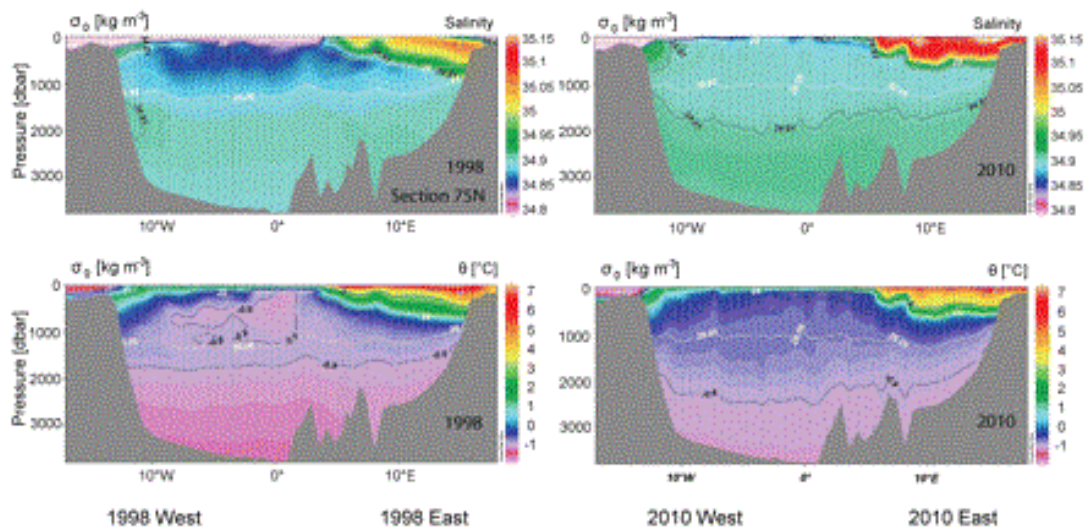


Figure 4: Salinity (upper) and potential temperature (lower) sections along 75°N in the Fram Strait, 1998 (left) and 2010 (right). Image from Rudels, et al. (2012).

1.3 Marine Isotope Stages (MIS)

In 1955, Cesare Emiliani did an isotopic analysis of marine cores from the Caribbean and the Atlantic (Gibbard & Lewin, 2016). In these isotopic results, he recognized 14 numbered “core stages”, in analogy to and for correlation with continental glacial stages (Railsback, et al., 2015). These came to be known as the Oxygen Isotope Stages (OIS) or the Marine Isotopes Stages (MIS). The MIS numbers are starting at “1” for the most recent age. It has been divided based on glacial or interglacial conditions, where odd numbers refers to interglacials (etc. 1, 5, 7), and even numbers to glacial (etc. 2, 4, 6). MIS 3, even though odd-numbered, is an interval no longer considered an interglacial (Railsback, et al., 2015). Further expansion were made for the isotope stages, when Shackleton (1969) divided the MIS 5 into 5 sub-stages, “a” through “e”. The division within the sub-stages were still the same, with “odd

letters” (a, c, e) being warm periods, and “even letters” (b, d) being cold periods (Shackleton, 1969).

Deep-sea sequences are being constructed from the remains of foraminifera that are preserved in the sediments, who build their tests by either CaCO_3 or SiO_2 . The oxygen isotope composition in these molecules varies in direct proportion of their surrounding water. They are dependent on that fact that, when continental ice builds up during glacial stages, the oceans are enriched in $\delta^{18}\text{O}$ (Gibbard & Lewin, 2016). This is because the lighter oxygen isotopes are more easily evaporated and ends up trapped in the glaciers on land. As a result, the oceans are enriched by $\delta^{18}\text{O}$, and the glaciers are depleted of it.

1.4 History of ice core drilling in Greenland

The first ice cores obtained in the 1950s were done by different research teams in Greenland, Antarctica and Alaska, but they had a generally low quality of ice recovery preventing any detailed analytical studies. According to Jouzel (2013), one can mark the years 1957-1958 as the starting point of ice core research (Jouzel, 2013). In 1961, two US army teams merged to form the Cold Regions Research and Engineering Laboratory (CRREL). They drilled several cores in Greenland and Antarctica, before they moved the drilling operation to Camp Century in northwestern Greenland, where the first ever continuous ice core to the bedrock was drilled, 1388 meters long. In 1968, the CRREL successfully drilled a 2164 meter long core at Byrd Station in Antarctica, but unfortunately the drill remained at the bottom and they had to wait until 1993 to again celebrate the success (Jouzel, 2013). Over this period, they teamed up with different teams from the University of Copenhagen and Bern led respectively by Willi Dansgaard and Hans Oeschger. Willi Dansgaard was a pioneer in the establishment of the close link between isotopic composition of polar snow and the temperature at the precipitation site, while Hans Oeschger, a specialist in low-level carbon-14 dating, was interested in dating the ice (Jouzel, 2013).

Following the success of the cores from Camp Century and Byrd, the Greenland Ice Sheet Project (GISP) was launched in the early seventies, focusing on deep drilling, defined as extending beyond the Last Glacial Maximum (LGM), 20,000 years ago. This eventually led to

the European Greenland Ice Core Project (GRIP) and the American GISP2.

Due to disturbances related to the proximity of the bedrock, neither of these cores provided reliable climatic information beyond 100,000 years. Since this was linked to the hilly relief of central Greenland, a zone located 200 km north of the GRIP was chosen from its flatter terrain, and in 1995, the North GRIP (NGRIP) international project was launched (Jouzel, 2013). The NGRIP drilling ended in 2003 at a depth of 3085 meters, producing climate records that extends back to 123,000 years before present (BP) (NorthGRIP community members, 2004).

The most important characteristic of the Greenland records deals with the existence of rapid climatic changes during the last glacial period and the last transition, called “Dansgaard/Oeschger” events (Jouzel, 2013).

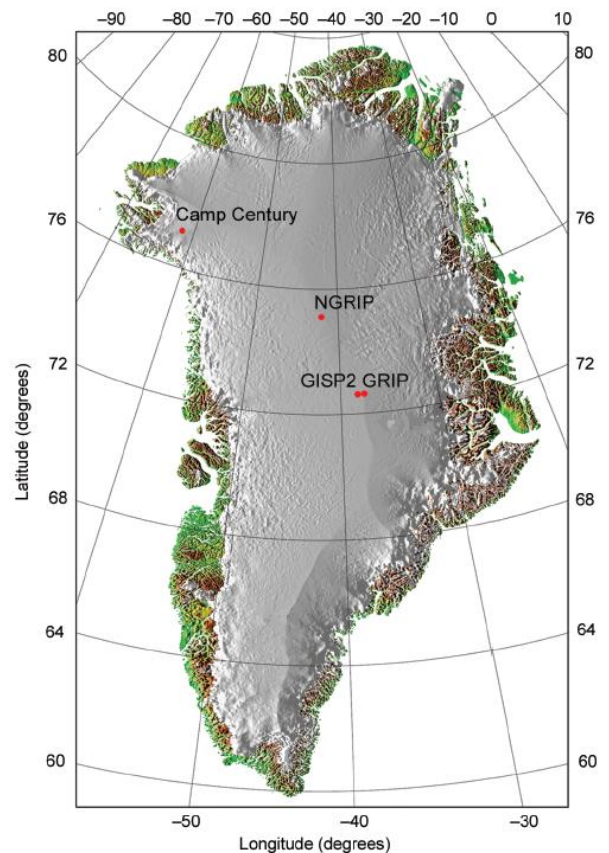


Figure 5: Locations of Camp Century, GISP2, GRIP and NGRIP. Picture taken from (NorthGRIP community members, 2004) (slightly modified)

1.5 Dansgaard/Oeschger Events

The rapid changes in $\delta^{18}\text{O}/\delta^{16}\text{O}$ in the Greenland ice cores were first described by Dansgaard, et al. (1982) and Johnsen, et al. (1992), and were eventually called Dansgaard/Oeschger events (D/O-event). These events are apparent in the ice cores as repeated transitions between warm interstadials and cold stadials (Barker, et al., 2015). The events start with a longer cooling event before dropping to its minimum temperature/ $\delta^{18}\text{O}$ level, eventually culminating in an abrupt shift to a warmer climate. The duration of each D/O-event varies a lot, with cycles lasting on average 10-15,000 years (Bond, et al., 1993). The interstadials lasted from 500 to 2000 years, and the irregularity in their occurrences are suggesting that the circulation of the North Atlantic Ocean were very complex (Johnsen, et al., 1992).

Bond, et al. (1993), found evidence that there are strong correlations between the ice records from Greenland and marine cores in the North Atlantic. The atmosphere and ocean surface were a coupled system, repeatedly undergoing massive reorganizations on timescales of centuries or less. At the abrupt cold-to-warm shifts that terminate D/O-cycles, rates of change in ocean temperatures must have been nearly the same as in the ice cores (Bond, et al., 1993).

Each cycle of the D/O-events culminated in a discharge of icebergs into the North Atlantic, and the largest of these events are known as the “Heinrich” events.

1.6 Heinrich Events

In 1987, Helmut Heinrich found massive amounts of ice-rafted debris (IRD) in cores from the North Atlantic, linking them to the climatic variations during the last glacial period. He found evidence that the cold-based foraminifera *N. pachyderma* (*s.*) and the IRD-events corresponded (Heinrich, 1988). Despite decades of study, Heinrich events are still not fully understood, mainly because the massive discharge of IRD occurred during the cold portion of the millennial-scale climate oscillations (Bassis, et al., 2017).

Heinrich (1988) argued that the major ice-rafting events were primarily controlled by the precession of the Earth’s axis, linked to a summer- and winter insolation minima which occurs two times during one precessional cycle (at angles 90° and 270°), giving enhanced events of ice-rafting on a mean period of $11,000 \pm 1000$ years (Heinrich, 1988).

Early theories also suggested that the Heinrich events were driven by internal instabilities associated with ice sheet flow, which are called “binge-purge” mechanisms (MacAyeal, 1993).

However, Bassis, et al. (2017), argued that explanations based purely on ice dynamics could not explain the synchronization of Heinrich events within D/O cycles. Bassis, et al. (2017), suggested that the Heinrich events were triggered by ocean forcing and modulated by isostatic adjustment (Bassis, et al., 2017). The theory is that there must have been an intrusion of warm subsurface ocean waters into the fjords, causing submarine melt, triggering the Heinrich events. Bassis, et al. (2017) made models that showed how Heinrich events could be triggered by relatively small millennial-scale fluctuations in subsurface

ocean temperatures (Bassis, et al., 2017).

What is certain is that the IRD events are a result of calving from the glaciers and that they are linked to abrupt climatic changes.

The Heinrich events can be used as a good calibration tool between cores in the North Atlantic, as most cores experience these events at the same time. Even though IRD can be used as a proxy in sediment cores, it can also cause disturbances for other proxies, like sortable silt.

1.7 Proxies in marine cores

1.7.1 Sortable Silt as a proxy

The currents in the deep ocean are the main controller of the particle transport and deposition in geological time, and have produced great muddy piles known as “drifts” Due to the high sedimentation rate in these drift, they have been used by paleoceanographical studies because they can offer higher resolution of the past ocean than the average for the world oceans (McCave, et al., 2017). These sediments are known as “contourites” as they are flowing along the topographic contours of the oceans, and because of the volume of the sediments they can contain records of the velocity of past deep ocean circulation (McCave, et al., 2017).

The knowledge about how the velocity in a current can transport, erode or deposit sediment have been known since Hjulstöröm published his “Hjulström curve” in 1935. This knowledge was at first applied to rivers, but as more research was done on ocean currents, one could apply similar calculations for the velocity of ocean currents. Ledbetter used the coarsening of the mean particle size in carbonate-free silt fractions to separate the high-velocity Antarctic Bottom Water (AABW) from the overlying, slower North Atlantic Deep Water (NADW) (Ledbetter, 1986).

McCave, et al. (1995a & b) worked on finding the optimal size fraction for the sortable silt, and found that the size fraction between 2-10 μm behaved cohesively like clay (McCave, et al., 1995a & 1995b). McCave found the size fraction 10-63 μm to be a good indicator for bottom current speeds. This is because silt coarser than 10 μm responds largely as single

particles to hydrodynamic forces on erosion and deposition because of the breakage of aggregates and is therefore size-sorted according to shear stress (McCave, et al., 1995b).

McCave, et al. (1995b) noted how bottom currents are usually not strong enough to transport sand-sized material. Hass (2002) further researched this. His basis was that the sand-sized material was predominantly ice-rafted, and made calculations based on the weight percentage of the sand and the mean size of the sortable silt. An ice-rafting calibration is necessary when dealing with sediments of the Nordic Seas, as much material during the last 1,000,000 years is originating from glaciers, and especially Heinrich-events would be very affected by the increased ice rafting.

There are also differences in how one do sortable silt analysis, each with different pros and cons. There are measurements using a sedimentation principle (e.g pipette method, Sedigraph), electrical sensing zone counters (Coulter, Elzone), and laser diffraction sizers (e.g. Fritsch, Coulter, Sympatek). While the measurements using sedimentation principle seems to be the most accurate, the electric sensing zone counters and the laser diffraction sizers might not “see” all the clay (McCave, et al., 1995b).

Bianchi, et al. (1999) did a comparison between the Sedigraph and a Coulter Multisizer, and found that the differences were minimal. However, the size fraction 0-63 μm should be measured with a Sedigraph, as the Coulter Multisizer cannot detect the complete distribution of the clay range.

The sortable silt methods can give good estimates of bottom current strength, and recent calibrations might even be able to give absolute speed estimations. McCave, et al. (2017) made calibrations for the mean sortable silt depending on the slope of the ocean bottom and the distance from the sediment source to make calculations to transform the sortable silt to speed estimates (McCave, et al., 2017).

Research in sortable silt have proven useful for palaeoceanographers as it can give estimates of past deep bottom current flows, and further research into this topic will lead to a better understanding of the deep ocean currents. Better modelling and understanding of the deep ocean currents and their effects on the global climate will eventually lead to better climate predictions.

1.7.2 Ice-Rafted Debris (IRD) as proxy

Ice rafted debris (IRD) found in marine sediments are interesting sedimentological parameters, providing information about factors such as distribution and number of icebergs, continental erosion by ice, sediment transport mechanisms and melt rate corresponding to water temperature (Grobe, 1987). IRD is mainly transported in two ways; by icebergs or by sea ice (ice floes). Hebbeln & Wefer (1997) wrote that sediments transported by ice floes generally contain less than 10% material $>63 \mu\text{m}$, while coarse material (sand and gravel) is commonly transported by icebergs. However, it has to be kept in mind that an increased input of coarse material implies increased amounts of fine IRD ($<63 \mu\text{m}$) supplied by both ice floes and icebergs (Hebbeln & Wefer, 1997).

1.7.3 Tephra as proxy

Throughout Earth's history, there have always been volcanic activity. The products from volcanic eruptions can provide good markers in sediment cores. Tephrochronology is the method of age determination that makes use of layers of volcanic ash (tephra). It involves the use of tephra layers that have spread out and covered large areas, making it able to do reliable correlations over long distances. Tephra horizons can be geochemically fingerprinted, using major element composition or trace and rare earth element compositions. They are therefore excellent to use for more precise correlations (Wastegård & Rasmussen, 2014).

As the volcanoes on Iceland are some of the most active in the world, they have produced large amounts of volcanic products scattered over the North Atlantic region. These layers are excellent for correlation, as they will be registered both in the marine cores and in the ice cores from Greenland (Davies, et al., 2014).

1.7.4 Foraminifera as proxy

Geologists find foraminifera useful due to their specific characteristics of the structure of their tests. After their first appearance in the Cambrian, foraminifera became abundant, and they still play a vital role in the marine ecosystem today. The foraminifera have an outstanding value in paleoclimatic, paleoenvironmental, paleobiological, paleoceanographic and zonal stratigraphy interpretation and analysis (Boudagher-Fadel, 2015).

Foraminifera usually build their test of either CaCO_3 or SiO_2 , both which contain oxygen isotopes, and can be used for $\delta^{18}\text{O}$ measurements, as mentioned in chapter 1.3.

These elements can also be substituted by other elements, which can be targeted to extract the specific information one might be looking for. For instance, many papers have used the Mg/Ca ratio in foraminiferal tests to calculate surface temperatures (from planktic forams) or bottom water temperatures (from benthic forams) (e.g. Ezat, et al., (2014 & 2016); Nurnberg, et al., (1996); Elderfield & Ganssen, (2000); Bryan & Marchitto, (2008)).

Knowledge of what environment certain foraminifera prefer can also be used as a marker of the conditions of the waters, like what current regime was present, the amount of nutrients, temperature and more (i.e. Rasmussen, et al., 1996a).

1.7.5 Magnetic Susceptibility as proxy

Magnetic Susceptibility has been used since the 1980s as a simple and rapid tool for reconstructing the paleoenvironmental records of deep-sea sediments. Lithological variations in deep-sea sediments may be climatically controlled by mechanisms like carbonate dissolution, productivity changes and dilution by terrigenous detritus. In the North Atlantic, deposition of glacial material from the base of melting icebergs is the most important mechanism for supplying terrigenous sediment to the deep seas, and is linked directly to climatic variations (Robinson, et al., 1995).

2 Methods and Materials

This study is mainly based on the lower end part of the piston core JM11-FI-19PC, going from 375 cm to 1105 cm. The upper end part of the core (5-85 cm) from Holocene (Ezat, et al., 2014) is also sampled as a reference to the Eemian interglacial.

Station	Date	Time (UTC)	Location	Latitude (N) Longitude (W)	Water Depth (m)	Recovery (cm)
JM11-FI-19PC	02.05.2011	16:12:52	Fugløy Ridge, Faeroe Islands	62°49'N 03°52'W	1179	1124

Table 1: Table containing information of the investigated core; JM11-FI-19PC.

The core has earlier been used by Mohammad Ezat for his 2014 article (Ezat, et al., 2014) and as most of the material from the work part of the core was used, the archive part of the core has been used for the sampling of material.

2.1 Materials from other sources

Much of the material used for this thesis is provided by Mohamed Ezat, who used the same core for his 2014 publication (Ezat, et al., 2014). Extra material was gathered from multiple sources consisting of benthic foraminifera data, magnetic susceptibility, bottom water temperatures from Ezat, et al. (2014 & 2016), planktic foraminifera data from Hoff, et al. (2016), relative sea level (RSL) from Grant, et al. (2012) and NGRIP data from Johnsen, (2004). The method will be presented here, while the results from the data will be presented in chapter 3.

2.1.1 Multi-sensor Core Logger

The magnetic susceptibility of the core was measured using a GEOTEK multi-sensor core logger (Ezat, et al., 2014). The core JM11-FI-19PC was measured every 1 cm.

Magnetic susceptibility (MS) measures the magnetization of the sediments in the core.

2.1.2 Foraminifera assemblage

~300 foraminifera had been identified and counted from the >100 µm size fraction at 5 cm resolution. Pristine foraminiferal tests from the foraminiferal benthic species of *M.*

barleeanus and *C.neoteretis* were selected for trace element and stable isotope analysis, and radiocarbon dates (Ezat, et al., 2014).

Tables were gathered from the supplements of M. Ezat's publication (Ezat, et al., 2014sup).

Stable Isotopes:

The stable isotope analysis had been performed using a Finnigan MAT 251 mass spectrometer with an automated carbonate preparation device at the Center of Marine Environmental Sciences (MARUM) at the University of Bremen (Germany) (Ezat, et al., 2014).

This analysis was used to get a $\delta^{18}\text{O}/\delta^{16}\text{O}$ relation.

Trace elements:

The foraminiferal test had been crushed and cleaned following the standard foraminiferal Mg/Ca cleaning protocol. The Mg/Ca values were converted to BWT (Bottom Water Temperature) using species-specific calibration equations (Ezat, et al., 2014).

Radiocarbon dates:

Radiocarbon dates had been measured on monospecific planktonic foraminiferal samples and calibrated using the Calib7.01 and Marine13 software programs (Ezat, et al., 2014).

The data for the main part of the core (375-680 cm) is collected from the supplements of the 2014 publication (Ezat, et al., 2014sup), and the data for the whole core dates are collected from the 2016 publication (Ezat, et al., 2016b).

2.1.3 North Greenland Ice-core Project Oxygen Isotope Data

The North Greenland Ice Core Project (NGRIP) gives a good insight in the climate of the Northern Hemisphere, stretching from the Eemian period to the present. The NGRIP has

produced oxygen isotope data reaching back to 123,000 years BP. Data from the NGRIP has been used to correlate the oxygen isotope dating with the core JM11-FI-19PC (Johnsen, 2004).

2.2 Sediment Coring

The core JM11-FI-19PC is a piston core, which differs from a gravity corer in that it can in a safer way take a longer core. As the piston corer penetrates the seafloor, a piston inside the corer stops at the sediment surface. The action of a piston creates a pressure differential at the top of the sediment column, which allows the soft material to enter the core liner without disruption. (WHOI, 2018)

JM11-FI-19PC penetrated 13 meters into the sediments. It retained 11.24 m of the sediment and was split into 11 sections. The upper 10 cm of the core was disrupted by “slushing”, and the first 10 cm of core #1 is empty.

The 11 sections were split into a work part and an archive part, then stored in the cooler at Fløyahallen, Tromsø, at ~4°C.

2.3 Sortable Silt

The sortable silt method is the main method used for this thesis. Sortable silt can be obtained by either a Sedigraph or by a Coulter Counter. In this thesis the Beckman Coulter LS 13 320 Laser Diffraction Particle Size Analyzer was used, which counts particles ranging from 0 to 2000 μm .

The “sortable” sediments are sediments of grain sizes that can be physically sorted by the bottom currents (Hass, 2002), which has been described to be the sizes from 10-63 μm (McCave, et al., 1995b). The reason the lower value is set to 10 μm instead of the 2 μm limit for silt, is because silt below 10 μm tends to have a cohesive behavior.

Sampling and method

17 samples were taken from the Holocene part of the core (5-85 cm) and 168 samples were taken from the main part of the core (375-1105 cm).

The samples were taken at an interval of every 5 cm. A small amount of sediment was scraped out and weighed, with the first part (375-790 cm) were to contain between 2-2.5g and the second part (795-1105 cm) were to contain 2.8-3.5g. The reason for this was to avoid losing too much of the older material due to the very possible input of larger amounts of IRD which would be removed from the samples. After the samples were weighed, they were put in tubes and marked, then left to dry for one day. Due to a slight difference in weight of all the tubes, the tubes were first weighed individually, then weighed with the samples to be within the given weight limits.

The tubes with the samples was then filled with a 20% HCl (hydrochloric acid) so the sample was covered. The HCl was added to remove any carbonate minerals from the sample (foraminifera etc.). Then the samples were left in a fume hood for 24 hours.

After the 24 hours, the samples was centrifuged for 4 minutes at 4000 rpm (rounds per minute), then washed with distilled water and centrifuged again. The washing of the samples was done twice, to ensure the removal of any excess HCl.

Next, the samples were applied with a 16.6% H₂O₂ (hydrogen peroxide) solution to remove any organic material. Same as with the HCl, the tubes were filled enough so that the samples were covered.

Error source: There was a misreading of the mixing tables, which resulted in the H₂O₂ to be mixed at the ratio of HCl, ending up in a slightly weaker solution for the first samples. The lab assistance assured me that this would not be a problem, but all further samples were applied with the same solution to avoid anomalies in the results.

As a result of this misreading, the first batch of samples (all from core #7 and the first 10 samples of #10) were done in reverse order, where they first was applied with H₂O₂, and then applied with HCl. Both my supervisor and the lab assistance doubted that this would have any visible effect on the results.

The tubes were then covered with aluminum foil with a hole in, so that the gasses from the

reaction could escape. They were then placed in a Thermal Bath at ~80 degrees C° for 2 hours. During the first 15-20 minutes, it was important to keep an eye on the samples, as most of the reaction took place during this period, and there was a risk of sediments boiling over. After the samples had been in the Thermal Bath for 2 hours, they were taken out and centrifuged for 4 minutes at 4000 rpm, washed with distilled water then centrifuged for 4 minutes again. The washing process was again repeated twice.

After the samples was centrifuged and washed, they were put in a new beaker with a lid. To get the samples out from the tubes, a small amount of distilled water was applied, and the tubes were shaken a few seconds on the test tube shaker.

After the samples were put in the new beaker, they were left to dry.

The dry samples were then put in plastic bags, gently crushed to remove coagulated particles, then about 0.2 g were put back in the beaker and applied with 20 ml of normal tap water.

The samples were then put on a shaking table for at least one day, to properly dissolve.

The dissolved samples were then first put in an ultrasonic bath for about 5 minutes. Samples that had not been properly dissolved were added 2 drops of Calgon, and then put in the ultrasonic bath. If they still were not properly dissolved, they were put back on the shaker table for some time.

The properly dissolved samples were put in the Beckman Coulter LS 13 320 Laser Diffraction Particle Size Analyzer and analyzed through three runs. All samples were poured through a 2 mm sieve, to avoid getting fragments above 2mm into the machine.

2.4. Ice-Rafted Detritus (IRD)

IRD was counted in the in the size fractions 150-500 μm and $>500 \mu\text{m}$. The samples were provided by Mohamed Ezat, who used the same core in his 2014 and 2016 publications (Ezat, et al., 2014 & 2016). The samples were already dry and sieved into fractions 100-1000 μm and had to be re-sieved into the preferred size fractions.

In the size fraction $>500 \mu\text{m}$ everything was counted. In the size fraction 150-500 μm , it was counted up to 300 grains. Some samples contained a lot and some samples contained very

little IRD. In these cases, it has been counted either more or less than 300 grains, but the goal was to get a decent average between the squares counted, to get a more accurate estimate of the amount of IRD grains in the sample.

The samples were weighed in the bottle (without the cap) before and after counting, and the values were subtracted to find the total weight of the counted sample. Total dry weights of the whole samples were provided by M. Ezat.

The samples were calculated to show IRD per gram of sediment.

2.5. Tephra

Tephra was counted mainly to identify known tephra layers. The tephra was counted additionally to the IRD, so the counting of the tephra occurred within the same number of squares that the IRD was counted on, and not set to a specific number of grains. The tephra counted was mainly basaltic.

Tephra layers were also counted and identified by M. Ezat, and will be used for comparison (Ezat, et al., 2014sup)

3. Results

This chapter will present the results gathered from the investigation of the core JM11-FI-19PC. The results produced by the author consists of the Sortable Silt (SS), IRD- and tephra counts, as well as the sand and clay count from the Coulter Counter. The sand count has been used to calibrate the sortable silt graph, using a calibration equation from Hass (Hass, 2002). In addition, the sortable silt graphs have been transferred into velocity (cm/s) to get an idea of the speed differences. The velocity calculations are not necessarily accurate for the Faeroese shelf, but calculated from the Iceland absolute overflow speed (McCave, et al., 1995b), and should give an estimate of the top and bottom velocities of the bottom currents passing over the core location.

3.1 Results used from other sources

Data has been gathered from multiple sources to be compared with the results found below. Most used are the data supplied by M. Ezat, containing magnetic susceptibility, benthic $\delta^{18}\text{O}$ data (Figure 7-10), age correlations (Table 3), $\delta^{13}\text{C}$ data and estimated bottom water temperatures (BWT) (see Figure 30 in chapter 4.3.2) (Ezat, et al. 2014 & 2016). Planktic $\delta^{18}\text{O}$ data and age calibration data have been gathered from Hoff, et al. (2016) (Figure 7-10). Data from the North Greenland Ice Core Project (NGRIP) have been collected from the National Oceanic and Atmospheric Administration's (NOAA) websites, contributed by S.J. Johnsen (Figure 25) (Johnsen, 2004).

Relative Sea Level (RSL) data have been gathered from Grant, et al. (2012) (Figure 32).

These results and comparisons will be used in chapter 4.

3.2 Sortable Silt

The sortable silt has been split into 3 main units, based on the activity of the bottom water currents (Figure 6). The main part will be between 375-695 cm in the core, covering Heinrich event 4 through 6, and interstadials 6 through 18. This will be the part most thoroughly investigated, as this unit coincide with the data from the publications of M. Ezat on the same

core.

The second unit will go from 675-925 cm, while the third unit will cover 905-1105 cm and the 5-85 cm from the top of the whole core, to get a comparison between the Holocene- and Eemian-periods.

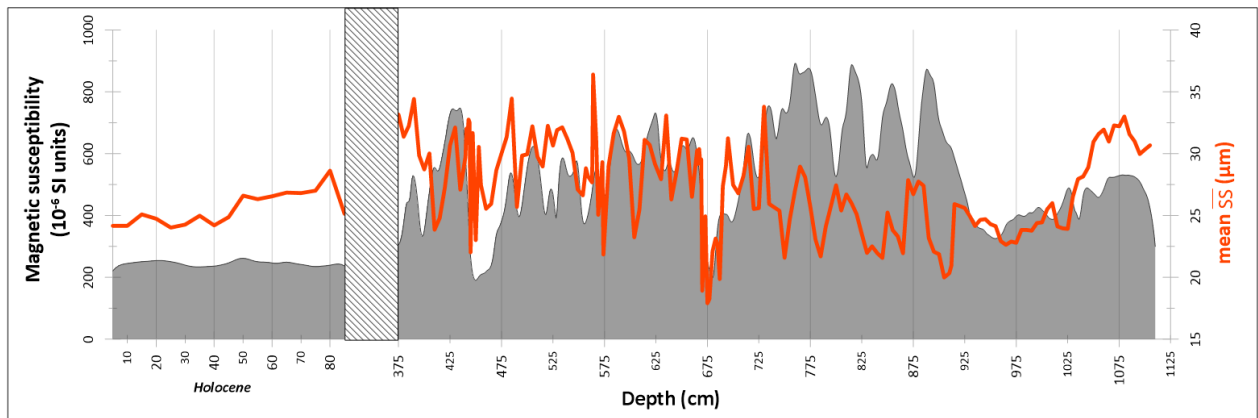


Figure 6: Sortable silt results for the investigated core. Mean \overline{SS} marked in orange. Magnetic susceptibility marked in gray.

3.2.1 Unit 1 (375-695 cm)

This unit shows five very low values and five very high values of silt mean size. The low values are found below 25 μm , while the high values are above 33 μm (Figure 7).

The general pattern from the graph seems to go from a very low value, rising fast to a high value, then returning to a low value over a longer period.

The average mean size of the entire section is also the highest in the whole core, with average values of 28.8 μm . However, the fluctuations between high points and low points vary at a higher rate as well.

The lowest mean size in the whole core can be found at 675 cm, at about 17 μm . The extra samples showed some fluctuations happening within this low energy zone.

The low point at 675 cm has been used as a marker between unit 1 and 2, where they overlap for 20 cm.

3.2.2 Unit 2 (675-930 cm)

Starting at 930 cm the unit have a very flat curve for the first 15 cm, slowly increasing the mean size by barely 1 μm over the first 4 data-points. At 915 cm there is a sudden drop of

about 6 μm , from 26 to 20 μm , reaching the second lowest mean size of this unit for 200 cm, at 905 cm in the core. From this point, it slowly rises back up to around 27 μm at 880 cm (Figure 8).

Unlike the first unit, this shows a slight trend of rapid decreases in mean size, and gradual increases.

At 915, 870 and 850 cm all points decrease drastically in mean size, and thereafter slowly increases.

The average mean size of the section is 24.7 μm , and unlike the first unit (375-695 cm), there are not that many big fluctuations in the mean size.

The unit overlaps with unit 1 from 695 to 675 cm, showing the lowest point in the core, to compare with the rest of unit 2.

3.2.3 Unit 3 (905 – 1105 cm)

This unit starts at 1105 cm with a decently high silt mean size, staying about 30 μm from 1105 cm to 1050 cm. Unlike the two earlier units, there are no abrupt jumps in \overline{SS} , and the graph seems to show very smooth curves compared to the other two section.

From 1050 cm the mean size of the silt decreases gently, from above 30 μm down to about 25 μm , where it stabilizes for about 110 cm down the section, from 1025 to 915 cm.

The two points worth mentioning in these 140 cm happen at 935 and 1010 cm, where at 1010 cm there is an increase in mean size of 1, and at 935 where there is a slight decrease in mean size. The differences in mean size is not big, but they stand out compared to the either gently increasing, or gently decreasing trends of the curve (Figure 9).

From 930 cm the graph is overlapping with unit 2, going from a gentle, increasing curve, into a plunge in mean size. The mean size decreases with about 6 μm from 915 to 905 cm, before it increase again.

3.2.4 Unit 4 (5-85 cm)

As expected from this unit it has a very stable graph, with an average mean size of 25,5 μm . It starts from 85 cm with an increase in mean size, then decreases a bit, before stabilizing around 25-26 μm . There were only slight differences in the \overline{SS} , so the scale was made smaller to enhance the variations in the graph (Figure 10)

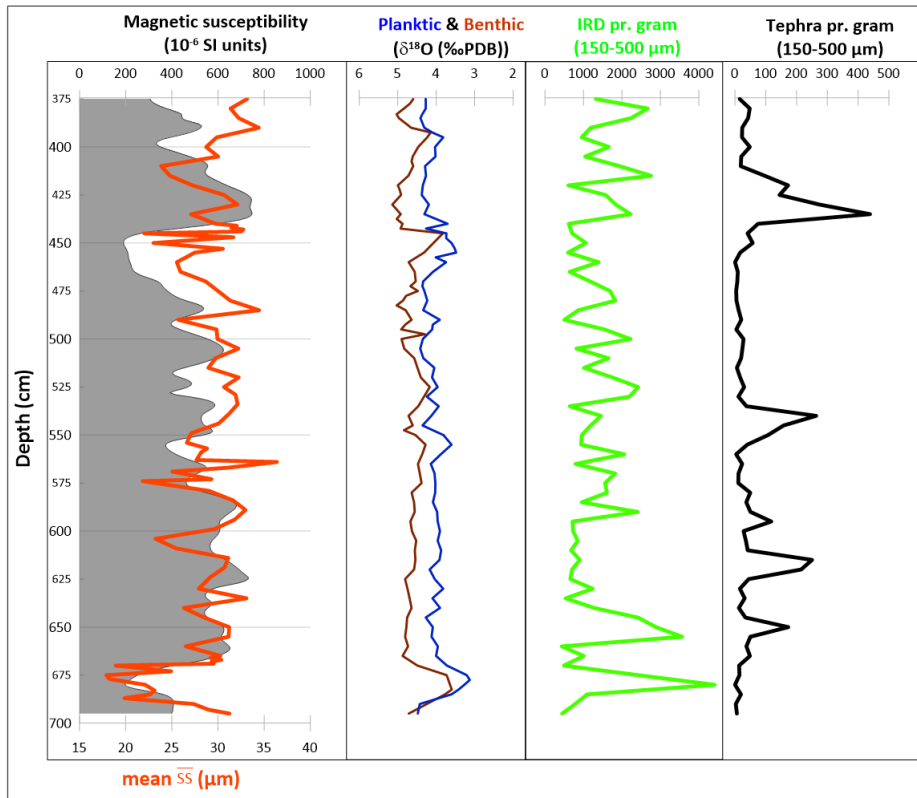


Figure 7: Unit 1; Sortable silt (orange), Planktic and Benthic $\delta^{18}\text{O}$ values (blue and brown), IRD pr. gram (green) and tephra (black)

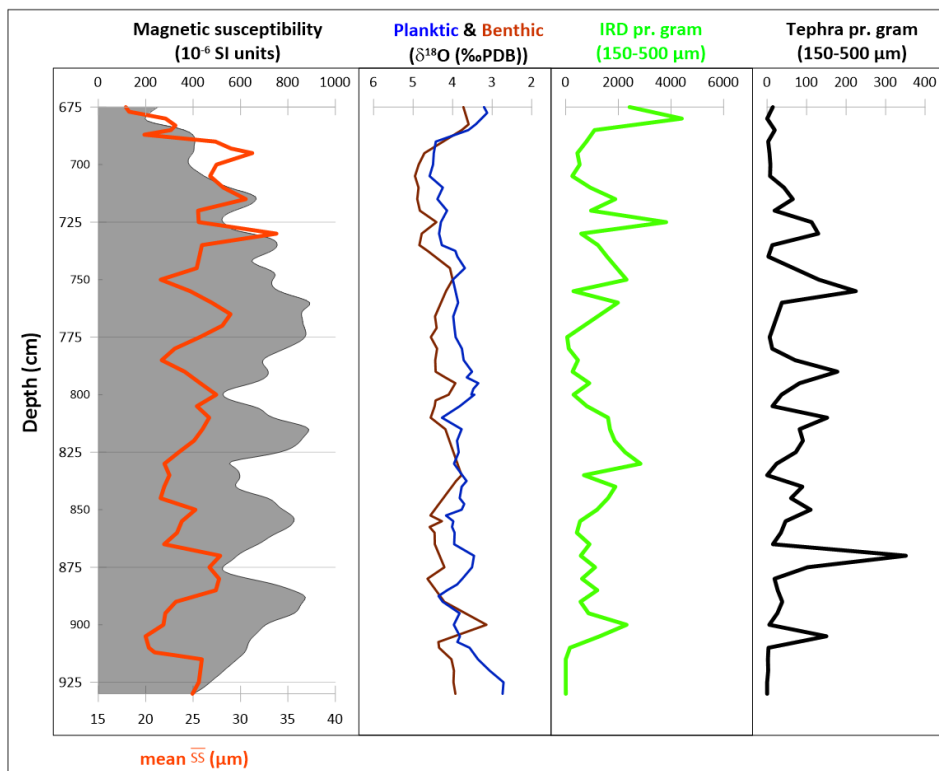


Figure 8: Unit 2; Sortable silt (orange), Planktic and Benthic $\delta^{18}\text{O}$ values (blue and brown), IRD pr. gram (green) and tephra (black)

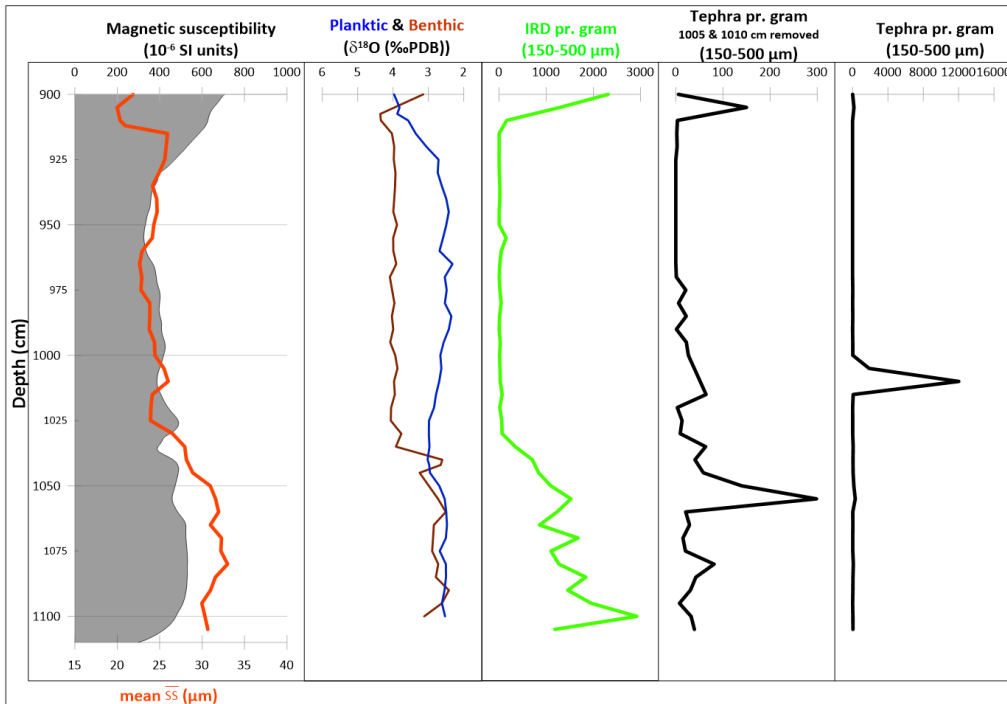


Figure 9: Unit 3; Sortable silt (orange), Planktic and Benthic $\delta^{18}\text{O}$ values (blue and brown), IRD pr. gram (green) and tephra (black)

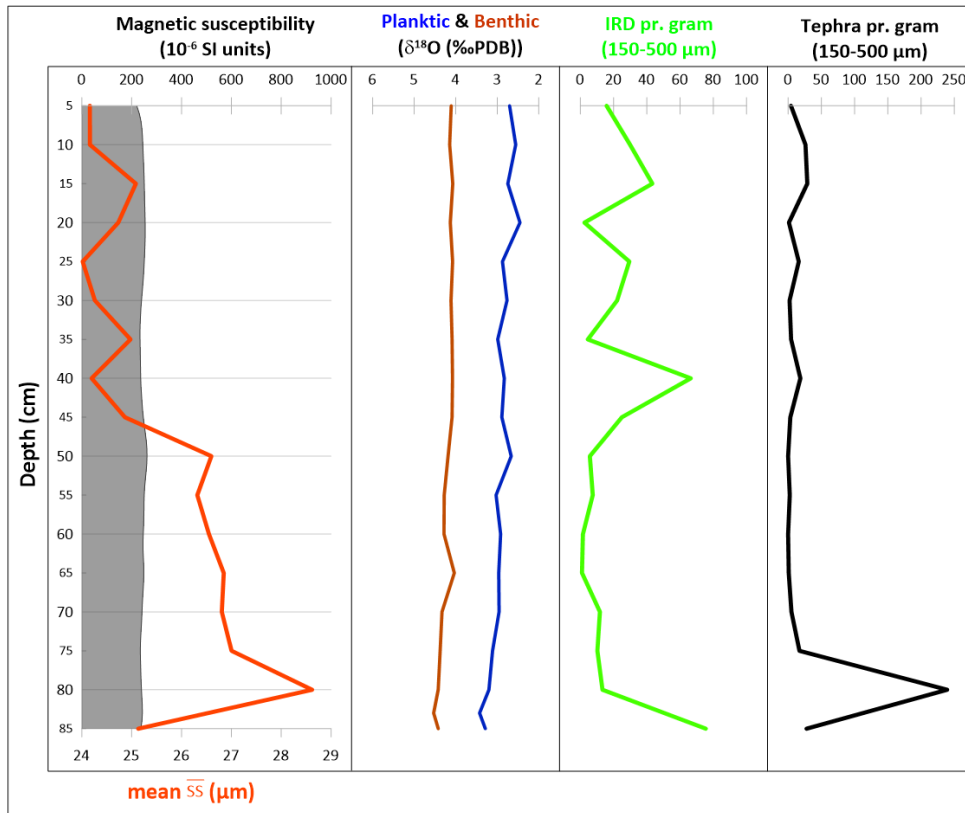


Figure 10: Unit 4 (Holocene); Sortable silt (orange), Planktic and Benthic $\delta^{18}\text{O}$ values (blue and brown), IRD pr. gram (green) and tephra (black)

3.3 IRD – Ice Rafted Detritus

The IRD counts have been split up into the same units as the Sortable Silt, to make it easier to connect the big IRD events with the SS-units. The individual units are linked up with the sortable silt, while all IRD counts are found below (Figure 11). As the >500 µm IRD only amplified the 150-500 µm, only the 150-500 µm has described and been used in the sortable silt units.

There was one error source in Unit 2, where 3 bottles of material were not found.

3.2.1 Unit 1 (375-695 cm)

The average IRD count of this unit is around 1405 IRD/g. Two large peaks can be found at the start of the unit, at 680 and 655 cm, with peaks at about 4400 and 3500 IRD/g. There is a period of low IRD counts, going from 620 to 595 cm, where the average lies around 750 IRD/g. The general pattern of the core is that there are sharp amplitudes swings at short intervals. It contain the biggest variability in the IRD count of all the units, and displays a saw-tooth graph. This corresponds well with the \overline{SS} of the same unit having the highest amplitude frequency (Figure 7).

3.2.2 Unit 2 (675-930 cm)

The average IRD count is smaller in this unit than in the previous one, averaging at 1100 IRD/g.

Starting from 930 cm, there are practically no IRDs to be found. A larger peak is found at 900 cm, going into a sig-sag pattern of smaller IRD releases between 890-860. A large and longer IRD event is happening between 860-810 cm.

As mentioned above, three samples are missing; 745, 765, 770 cm. There are indications that there are some bigger peaks at these points, where the adjacent data points are pointing upwards. The largest peak in this unit is found at 725 cm, at about 3800 IRD/g (Figure 8).

3.2.3 Unit 3 (905-1105 cm)

Unit 3 contains barely any IRD content between 910-1030 cm. There is a slight increase at 955 cm, but it barely records 150 IRD/g. The bottom of the core is showing bigger peaks,

with an average of 1400 IRD/g between 1040-1105 cm, and with the largest peak at 1100 cm containing 2900 IRD/g (Figure 9).

3.2.4 Unit 4; Holocene (5-85 cm)

The IRD count in this unit was very low. Some peaks within the Holocene are seen at 40 and 85 cm, but these barely contain 75 IRD/g, far below the values found in the lower part of the core (Figure 10).

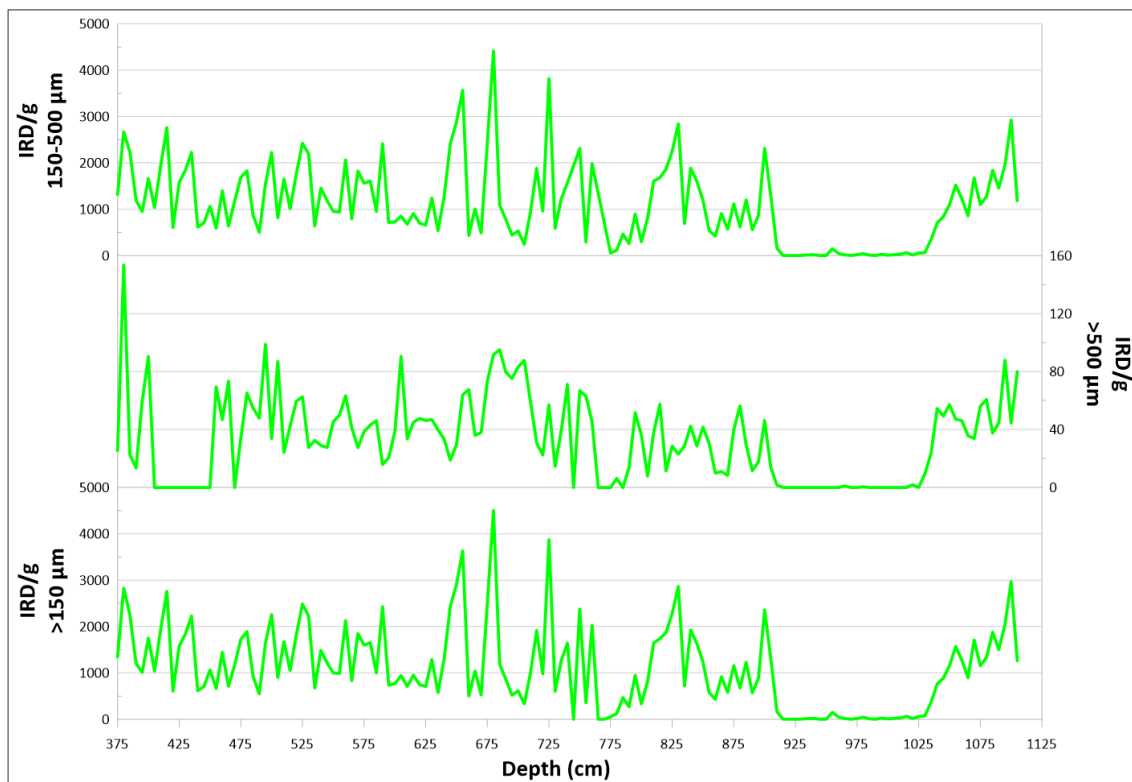


Figure 11: Results from all the IRD counts, showing 150-500 µm (top), >500 µm (middle) and all combined in >150 µm (bottom).

3.4 Tephra

The counting of tephra was done to find known tephra layers that could be correlated to the North Greenland Ice Core Project (NGRIP) and give a more accurate dating of the units (see chapter 3.7 and correlations in chapter 4). The individual units are linked up with the sortable silt, while all tephra counts are found below (Figure 12). As the >500 µm tephra

only amplified the 150-500 μm , only the 150-500 μm has described and been used in the sortable silt units.

3.3.1 Unit 1 (375-695 cm)

The first unit show 3 distinct peaks, at 435, 540 and 615-620 cm (Figure 7). These correlate to the layers M. Ezat found in his publication from 2014 (Ezat, et al. 2014a & 2014b).

The layer found at 435 cm should correlate to the Faraoe Marine Ash Zone III (FMAZ III), even though Ezat found this layer at 440 cm. The layer found at 540 cm correlates to the FMAZ IV, and the layer found at 615-620 cm correlates to the North Atlantic Ash Zone (NAAZ) II.

The FMAZ III layer difference by 5 cm compared with Ezat, et al. (2014) might be caused by the difference in the counting fractions. In this thesis the counts were done $>150 \mu\text{m}$, while M. Ezat counted $100 \mu\text{m}$. However, Hoff, et al. (2016) listed two depths for this layer; 427-428 and 438-439. This might be indicating that the layer is thicker than observed during the counting.

3.3.2 Unit 2 (675-930 cm)

Two peaks stand out on the graphs; at 755 cm and at 870 cm (Figure 8). The two peaks can be correlated to the layers Ezat found in his 2016 publication. These layers should correlate to the 5a-Top/BAS at 755 cm and the 5c-Midt/BAS at 870 cm (Ezat, et al., 2016a).

Several smaller peaks can be seen in the unit as well. Two small peaks above the 755 cm-layer, and 3 medium sized peaks between the layers at 755 and 870 cm. These are not known from earlier publications.

3.3.3 Unit 3 (905-1105 cm)

In this unit one peak stands out massively compared to the rest at 1005 and mainly 1010 cm. This layer should correlate to the 5e-Low/BAS that M. Ezat found (Ezat, et al., 2016a). Two other tephra layers were found at 905 and 1055 cm, but these have not been identified in earlier publications (Figure 9). The 5e-Midt/RHY has not been counted but included based on the findings of Ezat, et al. (2016).

3.3.4 Unit 4; Holocene (5-85 cm)

Once again there was very little to be noted in unit 4, and the scale have been reduced to find the variations. One layer is peaking at 80 cm (Figure 10). This layer is probably the Saksunarvatn tephra Ezat found at 83 cm (Ezat, et al., 2014a & 2016a)

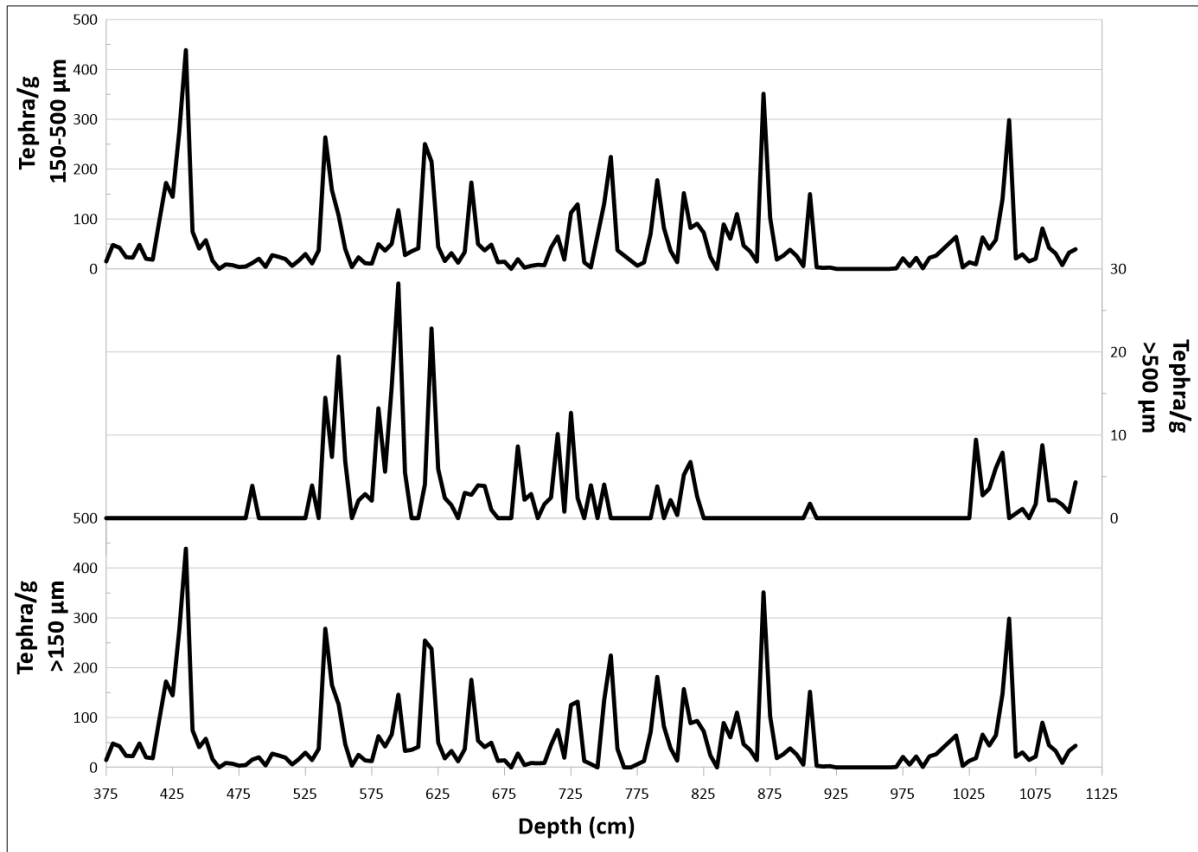


Figure 12: Results from all the tephra counts, showing 150-500 μm (top), >500 μm (middle) and all combined in >150 μm (bottom).

3.5 Sand Calibration

Bottom currents are rarely strong enough to transport sand grains. Using this information, we can assume that much of the sand-sized material in the core might be transported by ice. Knowing that material have been transported to the location by ice rafting, it must also be expected that a part of the silt and clay fraction also have been deposited like this.

The sand calibration is a way to try to remove the ice-rafted material from the measured silt fraction, using a calibration from Hass (Hass, 2002).

Scatter plots were created to find the right equations (Table 2).

The sand calibration has been done for each unit (Figure 13-17). This is mainly to avoid to big differences in the graphs, as the sand content in the different units are very different.

Especially unit 3 and the Holocene unit made some difficulties, due to the differences in sand content. Unit 3 have been split from 1030 cm into two calibrations, based on the very low amount of IRD found between 1030-910 cm (Figure 9).

After trying to eliminate distorted values given by skewed sand contents or low IRD-counts, these were the equations used;

UNIT	Y	R ²
1	$25,29x^{0,0479}$	0,398
2	$19,111x^{0,1406}$	0,68
3 (below 1030 cm)	$20,007x^{0,1009}$	0,481
3 (above 1030 cm)	$15,048x^{0,2675}$	0,8358
Unit 4 (Holocene)	$18,071x^{0,1374}$	0,4807

Table 2: Scatter plot equations for all units.

Where:

- $Y = \overline{SS}_{pot}$ (potentially ice-rafted sediment)
- $X =$ Sand content in wt%

These were used to calculate the $\Delta\overline{SS}$, given as;

$$\Delta\overline{SS} = \overline{SS} - \overline{SS}_{pot}$$

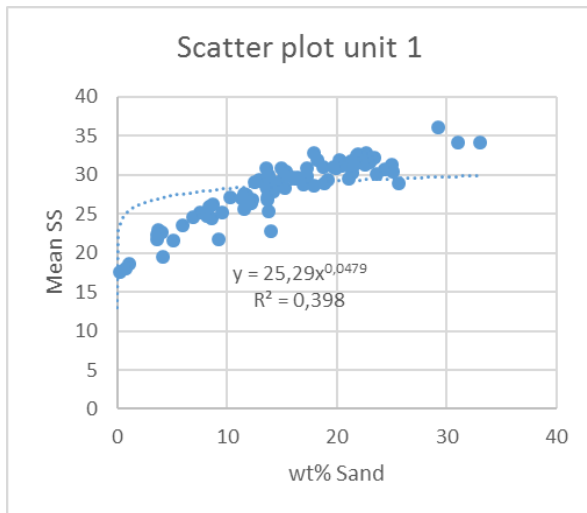


Figure 13: Scatter plot for unit 1

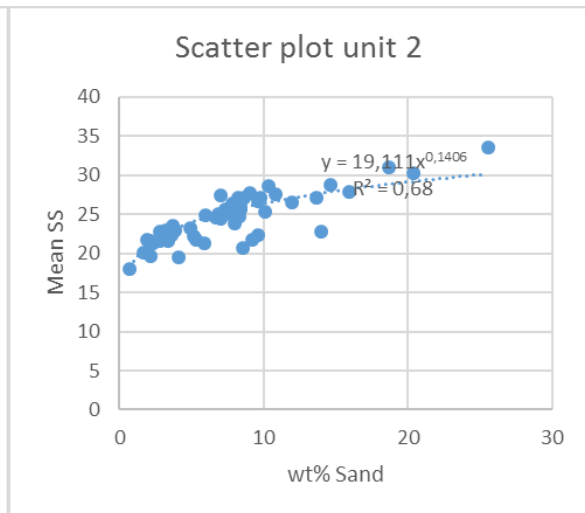


Figure 14: Scatter plot for Unit 1

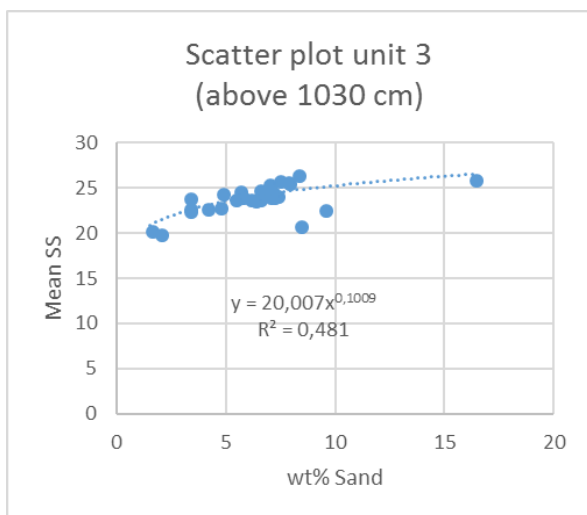


Figure 15: Scatter plot for unit 3 (below 1030 cm)

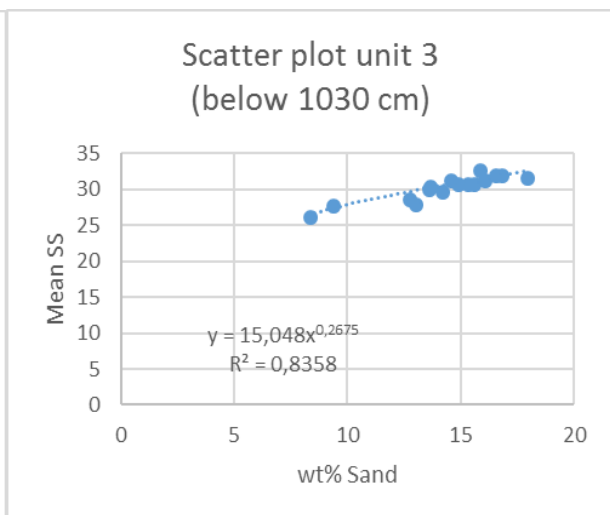


Figure 16: Scatter plot for unit 3 (above 1030 cm)

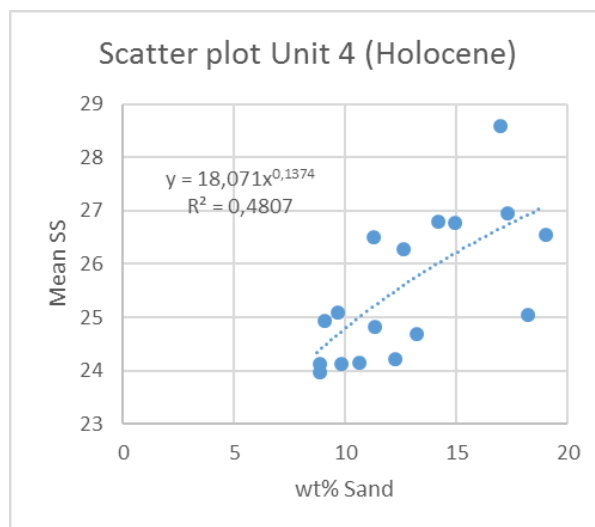


Figure 17: Scatter plot for Unit 4 (Holocene)

The values given by the $\overline{\Delta SS}$ shows current speed either increasing or decreasing (Figure 18- Figure 21).

The Holocene results might be unnecessary to calibrate, as the IRD content is almost non-existing in this unit (Figure 10).

The calibrated $\overline{\Delta SS}$ will be discussed more in the next chapter.

The sand, silt and clay ratios show generally high content of silt throughout the whole core (Figure 22).

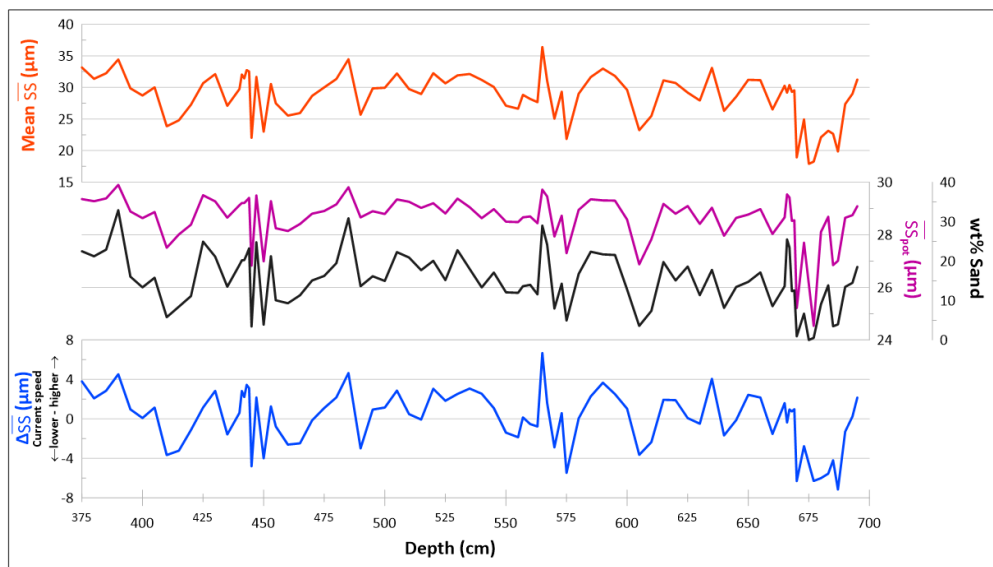


Figure 18: Sand calibration for unit 1.

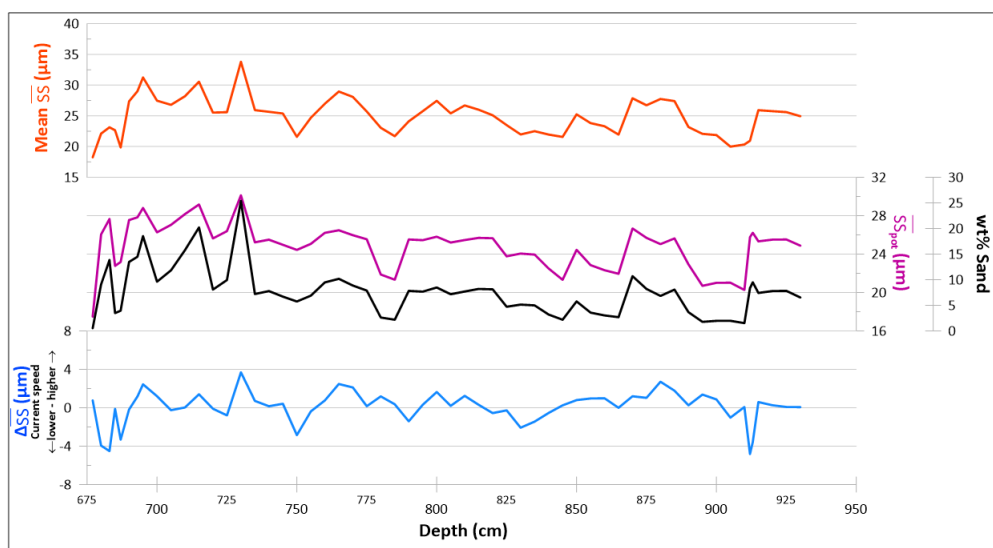


Figure 19: Sand calibration for unit 2.

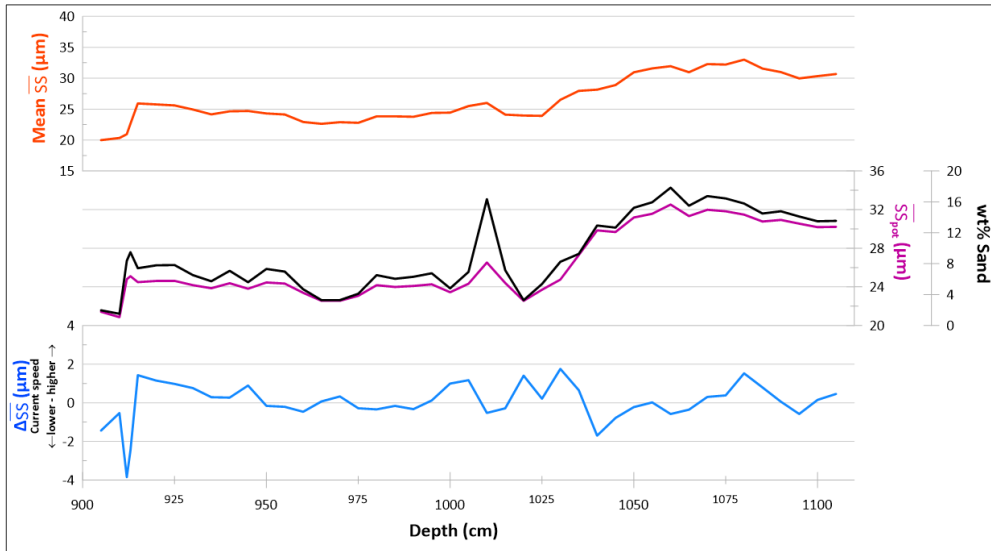


Figure 20: Sand calibration for unit 3

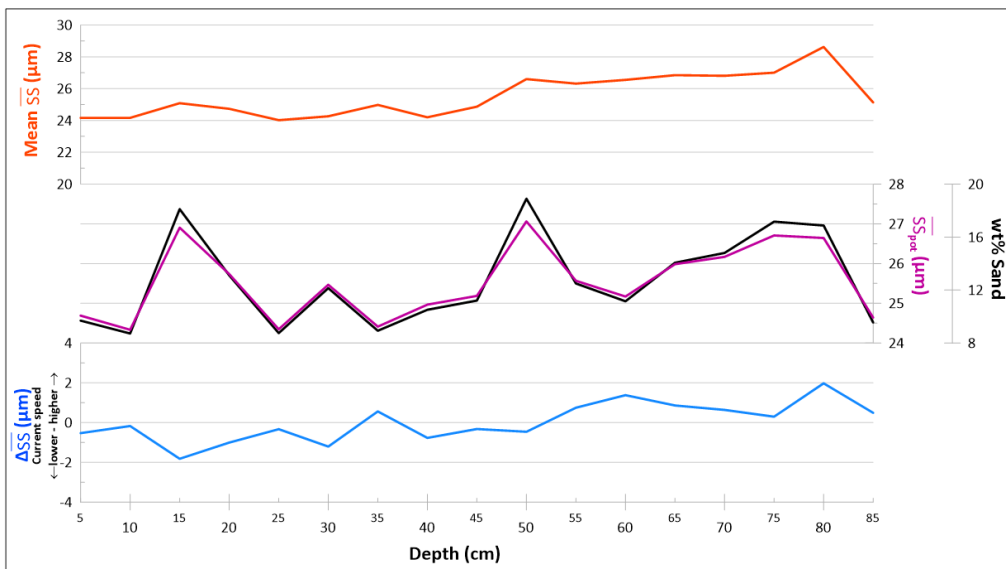


Figure 21: Sand calibration for unit 4 (Holocene)

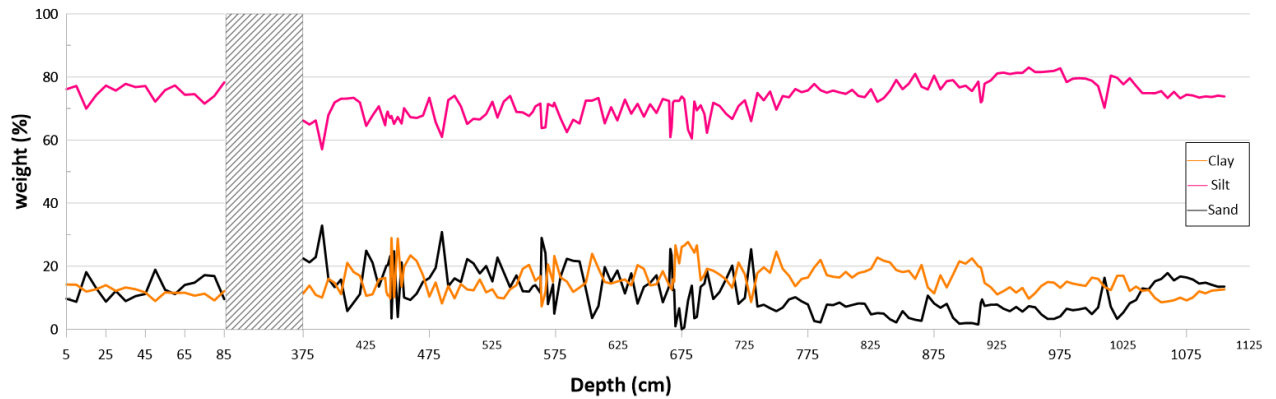


Figure 22: Sand, silt and clay percentages throughout the core JM11-FI-19PC.

3.6 Velocity estimates

The sortable silt alone does not give a certain estimation for the velocity of the bottom water currents. This subsection presents a possible estimate of the velocity, using the Iceland overflow region absolute calibration equation from McCave (McCave, et al., 1995b). The Iceland overflow equation is used as it is in closest proximity to the Faraoe-Shetland Channel, and should share some similarities.

The equation is gives as;

$$U = 1.31\overline{SS} - 17.18 \text{ cm s}^{-1}$$

It must be pointed out that these velocities are not absolute or certain, but are meant to give an approximate difference in the velocities between the high and low values of mean silt size found in the sortable silt graphs (Figure 23)

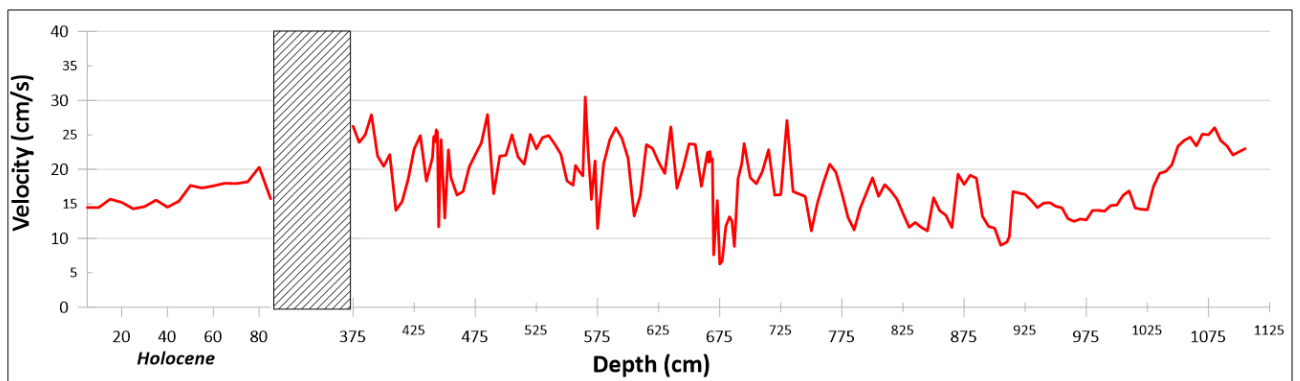


Figure 23: Estimated velocity graph, based on the Iceland overflow absolute calibration equation (McCave, et al., 1995b).

3.7 Construction of the age model

The age-depth plot (Figure 24) and the age model (Figure 25) for the core has been done by taking the average sedimentation rate between known ages in the core, giving a year/cm equation. The ages are taken from the tephra layers and from interstadial onsets, provided from Hoff, et al. (2016) and Ezat, et al. (2014b) (Table 3). The age model has the last known age at 127.000 years, but based on the assumption of Ezat, et al. (2016), the end of the core have been set to 135.000 years, and calculations have been done between the last certain tephra layer to this age (FIG) (Ezat, et al., 2016a).

The Marine Isotope Stages (MIS) have been dated from Hoff, et al. (2016), and substages within MIS 5 have been divided based on the publication from Railsback, et al. (2015).

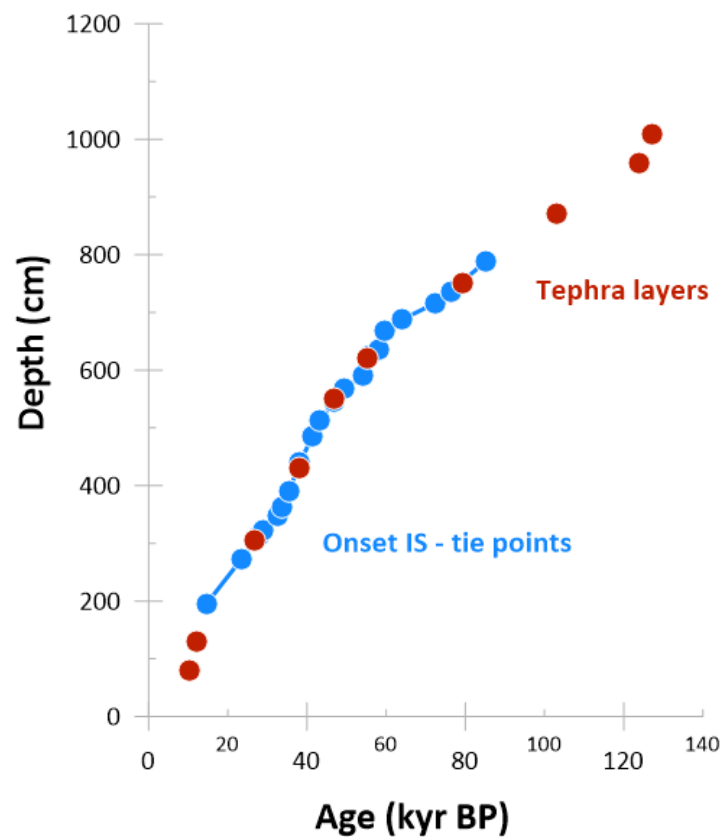


Figure 24: Age-depth plot with tephra layers and Onset IS - tie points. (See Table 3 for Tie points.)

Tie points: IS ONSET	age (kyr)	depth JM-FI-19PC (cm)
Sasunarvatn tephra	10,347	80
Vedde Tephra	12,171	130
Onset IS1	14,692	196
Onset IS2	23,34	272
FMAZ II	26,74	305
Onset IS3	27,78	313
Onset IS4	28,9	323
Onset IS5	32,5	348
Onset IS6	33,74	362
Onset IS7	35,48	390
FMAZ III	38,122	430
Onset IS8	38,22	441
Onset IS10	41,46	486
Onset IS11	43,34	513
FMAZ IV	46,8	543
Onset IS12	46,86	545
Onset IS13	49,28	567
Onset IS14	54,22	590
NAAZ II	55,38	620
Onset IS15	55,8	625
Onset IS16	58,28	637
Onset IS17	59,44	668
Onset IS18	64,1	688
Onset IS19	72,34	716
Onset IS20	76,44	737
5a-Top/BAS	79,3	750
Onset IS21	85,06	788
5c-Midt/BAS	103	870
5e-Midt/RHY	124	960
5e-Low/BAS	127	1010

Table 3: All data points used for the age-depth plot (Figure 24) and the age model (Figure 25). Tephra layers are collected from Ezat, et al. (2014 & 2016) and Hoff, et al. (2016). Onset IS ages and depths are collected from Hoff, et al. (2016).

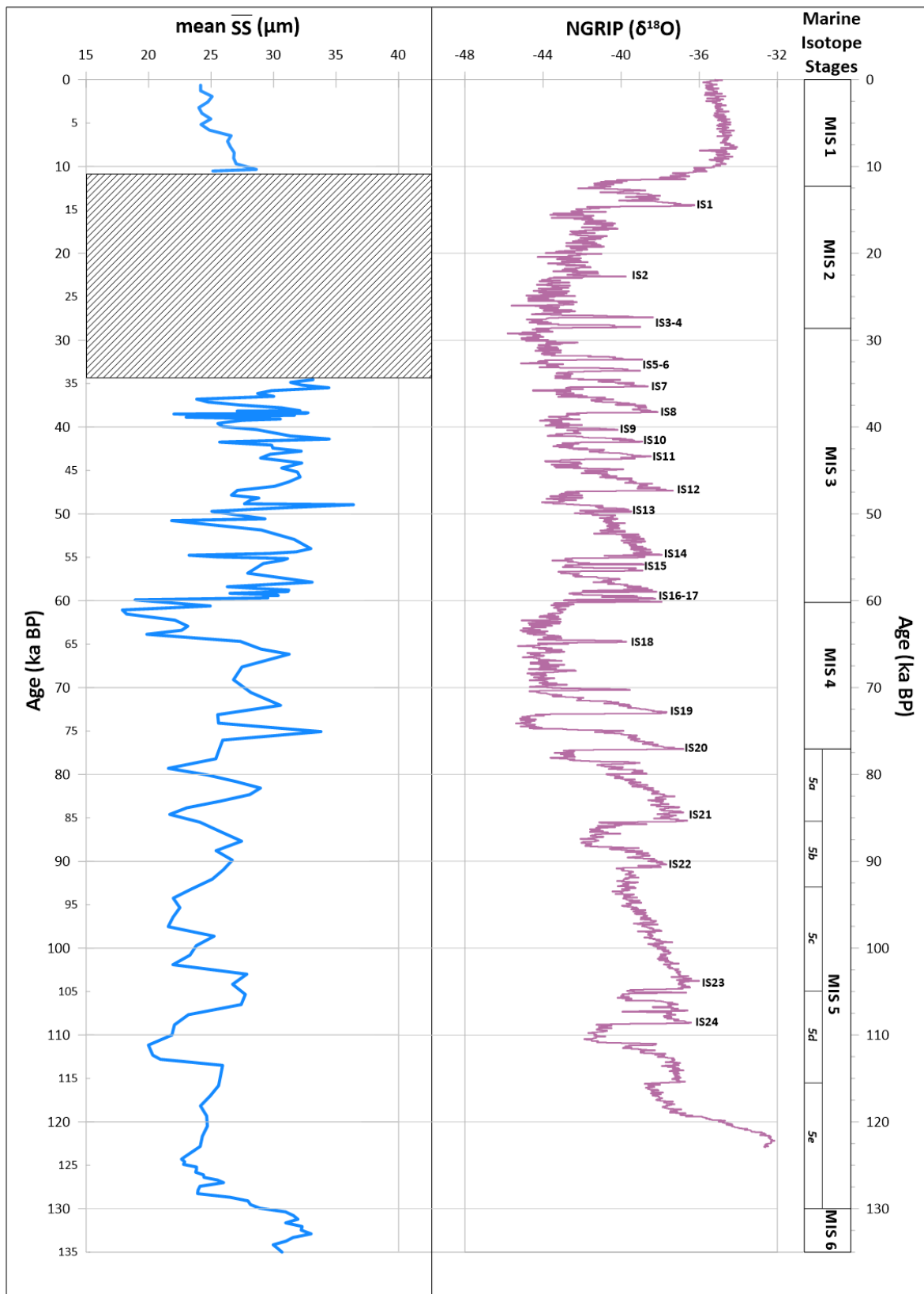


Figure 25: Age model for the core JM11-FI-19PC (blue) compared to NGRIP (purple). Values from mean sortable silt is used to create the graph from the investigated core. Striped area between ~35 - ~10 ka BP is the part of the core which have not been investigated.

4. Discussion

4.1 Interpretation and age correlation

4.1.1 Unit 1: 375-695 cm

Unit 1 is the section that contains the most data, as M. Ezat focused on the core up to this point in his 2014 paper (Ezat, et al., 2014). As seen in the results, this unit contains 3 known tephra layers, this being the Faeroe Marine Ash Zone III and IV (FMAZ III/IV) and the North Atlantic Ash Zone (NAAZ) II. With exception of the FMAZ IV, these layers are well known in the NGRIP (Ezat, et al., 2016a), and can be correlated against it. The FMAZ IV is discussed by Wastegård and Rasmussen and have been dated to $46,800 \pm 1000$ years BP (Wastegård & Rasmussen, 2014).

This dating gives an approximate correlation to the NGRIP, and places Unit 1 between interstadial 7 through 18 (Figure 26). That would also mean it contains Heinrich events 4-6 (H4-6), found below interstadials 8, 12 and 17 in the NGRIP (Bond, et al., 1993) (Bond, et al. used GRIP, but correlations to the interstadials should be the same).

The Heinrich-events are found around 450 cm (H4), 550 cm (H5) and 675 cm (H6). This also correlates with the sortable silt results, where all H-events show high \overline{SS} before the event, then a steep fall in mean size, before rapidly increasing in size. The oxygen isotopes from Hoff and Ezat (Ezat, et al., 2016a) (Hoff, et al., 2016) also show low values of $\delta^{18}O$ around these depths, indicating an influx of fresher water, most likely from meltwater. This is a strong indication for the Heinrich events (Hoff, et al., 2016).

The big IRD event at 680 cm in the core would solidify a Heinrich event happening at this interval.

The $\Delta\overline{SS}$ values do not differ much from the mean \overline{SS} values (Figure 18). It might seem as the high \overline{SS} values are a result of ice-rafted silt biasing, but the $\Delta\overline{SS}$ is showing similar current speed increases. However, the big differences in sand content between the interstadials and stadials might weaken the validity of the $\Delta\overline{SS}$ -graph.

4.1.2 Unit 2: 675-930 cm

Unit 2 overlaps with Unit 1 at the H6-event and starts at interstadial 18. As seen from Figure 7, there are multiple tephra layers that have been counted. Not all of these tephra layers can be correlated to the NGRIP, which makes this unit harder to date with certainty. From the results, it was concluded that two of the tephra layers are 5a-Top/BAS (755 cm) and 5c-Midt/BAS (870 cm). This would place these two tephra layers at ca. 78.5-80.1 ka BP and ca. 104-106.5 ka BP in the NGRIP (Davies, et al., 2014). This would indicate that Unit 2 stretches from interstadial 18 to interstadial 24 (Figure 26).

Unit 2 contains Heinrich events 6 through 10, however not all can be placed with certainty. Heinrich event 8 should be at around 800 cm. This is consistent with M. Ezat, as well as it correlates with oxygen isotopes and sortable silt (Figure 26) (Ezat, et al., 2016a). Heinrich event 7a and 7b should be found below interstadials 19 and 20 (Rasmussen, et al., 2003). There is some uncertainty to where these events can be found in the oxygen isotope graph, but there are indications that they can be placed around 725 cm and 740 cm. This also fits well with them being on each side of the high sortable silt value found at 730 cm, and with a following peak at 715 cm (Figure 26). This also correlates with a big IRD event at 725 cm, and a smaller IRD event around 745 cm (Figure 8).

The remaining two events, H9-10, are harder to place. According to Rasmussen, et al. (2003), H10 is taking place between interstadial 23-24, at the transition between MIS 5d and 5c (Rasmussen, et al., 2003). However, the results from the \overline{SS} -graph show a rapid decrease in silt mean size at 915 cm (Figure 8). The \overline{SS} results are pretty consistent with the apparent cooling between 110-115 ka BP when compared to the NGRIP (Figure 25).

In the oxygen isotope graphs both show an increasing $\delta^{18}\text{O}$ -value at this point, but at 900 cm the benthic $\delta^{18}\text{O}$ -values suddenly decreases rapidly. This is also consistent with a higher value of IRD found at the same point (Figure 8). Correlating the age and interstadial number towards the NGRIP, there is also found a sudden increase followed by a steep decrease in $\delta^{18}\text{O}$ -values. All this indicates at least similar conditions to a Heinrich event, and one can argue that H10 actually takes place here, after interstadial 24. In Figure 26, the H10-event is split into H10a and H10b, mainly based on the big fluctuations in the NGRIP and the $\Delta\overline{SS}$. The IRD peak at 905 cm might indicated that there was an IRD event here, but there is a

possibility that this only connects to H10a, and that H10b is not a true H-event. The sig-saw pattern following this IRD event might be a result of unstable climate, making the glaciers have pulsating calving episodes. The NGRIP is also showing a small cold event in the middle of IS24, indicating instability of the climate during this interval (Figure 26).

In this unit, the $\overline{\Delta SS}$ values can be used for a better correlation. The calibrated values have sharpened the curves, and especially interstadial 23 is probably more visible (Figure 8). Considering that the tephra layer at 870 cm is located on a high mean size \overline{SS} -value, it is plausible to believe that this is indeed the 5c-Midt/BAS described by Rasmussen (Rasmussen, et al., 2003), and also referred to by Davies as *5c-DO23i/BAS-I* (Davies, et al., 2014). This would solidify its age of around 103 ka BP, placing interstadial 23 at this depth (Figure 26). If the placement of the tephra layer at 870 cm is correct, then the $\overline{\Delta SS}$ -graph could be showing the brief cold event Rasmussen, et al. (1999) mentioned, at 865 cm in the investigated core (Figure 26). This correlates well with a slightly increased IRD content at this point as well, just after the tephra layer. Rasmussen et al (1999) found the IRD increase and the tephra layer at the same depth in core MD95-2009, so it is a good indication that this interpretation is correct. This would then lead into a longer period of cooling before H9, which after correlating IRD content, $\overline{\Delta SS}$ and $\delta^{18}O$, should be placed between 815-830 cm (Figure 26).

As mentioned in the results, there are indications of some other layers within this unit that was not identified by Ezat et al (2014 & 2016).

The two first are found at 715 cm and 725-730 cm. They do not stand out as much as the others do, but if the interstadials and H-events 7a and 7b have been interpreted correctly, one can find tephra layers that are located during these intervals in the NGRIP. Davies, et al. (2014) describes two layers in the NGRIP as *4-DO19i* and *NGRIP-2548.35 m*, dated at ca. 72.6 ka BP and 74.2 ± 1.652 ka BP. As the 4-DO19i is referring to interstadial 19 it is also found here in the NGRIP, while the NGRIP-2548.35m is referred to as "*being deposited close to sharp cooling transitions*" (Davies, et al., 2014).

This fits surprisingly well with the high mean size of the \overline{SS} at 715 cm, and the sharp drop in \overline{SS} from 730-725 cm. As said, this correlates surprisingly well with the NGRIP.

The third interesting layer, at 810 cm, that might be correlated to the NGRIP from the results

are referred to as *NGRIP-2742.85m* and *NGRIP-2745.60m* by Davies et al (2014). These are dated to 89.7 and 89.9 ± 2 ka BP, placing them on top of interstadial 22 and they should “*lie close to signals of rapid warming*” (Davies, et al., 2014). These layers also fit surprisingly well with the layer found in the results at 810 cm. Correlated with the \overline{SS} -graph it is also located at a peak in mean size, combined with being located right before H8.

However, this is nothing more than speculation without doing chemical analyzes of the tephra found at these depths, but it would certainly be interesting considering these layers contain close to the tephra counts found in e.g. 5a-Top/BAS.

4.1.3 Unit 3: 905-1105 cm

Unit 3 overlaps with Unit 2 in the part interpreted above to be H10, at its start at 905 cm. Two tephra layers are used for correlation in this unit; 5e-Midt/RHY and 5e-Low/BAS. 5e-Midt/RHY is based on the tephra layer described by M. Ezat (Ezat, et al., 2016a), while 5e-Low/BAS have been counted. These layers are found at ~960 cm (5e-Midt/RHY) and 1010 cm (5e-Low/BAS) (Figure 9).

5e-Low/BAS-IV is dated to ca. 127 ka BP, placing it at the start of the Eemian period, while 5e-Midt/RHY is dated to ca. 124 ka BP placing it in the middle of the Eemian period (Wastegård & Rasmussen, 2014). 5e-Low/BAS-IV corresponds to the increase in \overline{SS} at the same depth and adds an extra indicator for the start of the Eemian period.

From the start of the Eemian period at 1010 cm the \overline{SS} shows a slightly decreasing curve from 1010-965 cm, coinciding with the 5e-Midt/RHY tephra layer. From 965-915 cm the \overline{SS} is slightly increasing again, before it plunges down at 915 cm, entering what was interpreted in unit 2 as H10. This corresponds to a notably decrease in the in the $\delta^{18}O$ in the NGRIP (Figure 25).

The oxygen isotopes show a relatively stable curve from 1035-915 cm. The benthic $\delta^{18}O$ -values are stable around 4‰ from 1035-915 cm, while the planktic curve is slightly decreasing from 1035-965 cm, then increasing from 965-900 cm (Figure 9).

Combining the \overline{SS} -graph and the oxygen isotopes, are indications that during the first half of the Eemian period there was a general warming, while during the second half the climate was starting to cool. The planktic $\delta^{18}O$ -values is decreasing in the first half, when one could expect meltwater coming from inland glacier remains from the Saale ice age. The increase in

$\delta^{18}\text{O}$ -values from around 965 cm indicates a build-up of ice on land once more. This corresponds with the findings of Rasmussen, et al. (1999), who noted an indication of a colder climate from around 119 ka BP (Rasmussen, et al., 1999). Rasmussen, et al. (1999) also note the delay in the response of the deep-sea foraminiferal assemblages. This also correlates well with the $\overline{\text{SS}}$ -graph, as it is increasing from the same point as the interpreted cooling period, something that might be linked to the relative sea level, which will be discussed further down.

The $\Delta\overline{\text{SS}}$ graphs show some variations within the Eemian period. One of the features is that current speed increase from 1010 to 1005 cm, which should correlate well to the warm period in the beginning of the Eemian. Two current speed increases is also found at 1020 and 1030 cm. Rasmussen, et al. (1999) noted that there was some outflow pulses between the start of the Eemian and H11 (127-129 ka BP), and it might be these signals that are picked up by the $\Delta\overline{\text{SS}}$ graph.

The $\Delta\overline{\text{SS}}$ might be a bit more unreliable in this unit, as the sand values are very different between the glacials and interglacials, as mentioned in the results. Especially the $\Delta\overline{\text{SS}}$ -values from 1010 cm might be skewed, due to the high sand content at this depth.

The IRD counts show a large peak at 1100 cm, and then a sig-saw pattern with decreasing IRD content towards 1030 cm. Comparing with the benthic $\delta^{18}\text{O}$ -values, which have a small peak at 1060 and 1090 cm, it is probably correct to place H11 in this interval, as M. Ezat did (Ezat, et al., 2016a).

A relative big tephra layer was found peaking at 1055 cm, however this is not known from other sources.

4.1.4 Holocen: 5-85 cm

Ezat, et al. (2014) found the Saksunarvatn tephra at 83 cm in the core, which correspond well with the layer found at 80 cm (Figure 10). This places the bottom of this unit at approximate 10.5 ka BP.

Benthic oxygen isotopes show stable values at about 4‰, while the planktic have relative stable values at 2,5‰. This indicates that general bottom conditions were similar as today, and that the ocean circulation have in general had similar conditions since the end of

Younger Dryas (Rasmussen, et al., 2002). The \overline{SS} -graph show similar results, with a slight increase at 80 cm, then slightly decreasing towards present (Figure 10). With an average mean size of 25.5 μm , it is similar to the Eemian period, with an average of about 24 μm . These similarities will be looked more into further down.

The $\Delta\overline{SS}$ -curves for this unit (Figure 21) is showing bigger variability than the mean \overline{SS} -curve, but considering the low content of IRD found in this unit, it begs the questions for the necessity of the calibration being done on this unit. The overall pattern is still similar, with a general decline in current speed towards present day conditions.

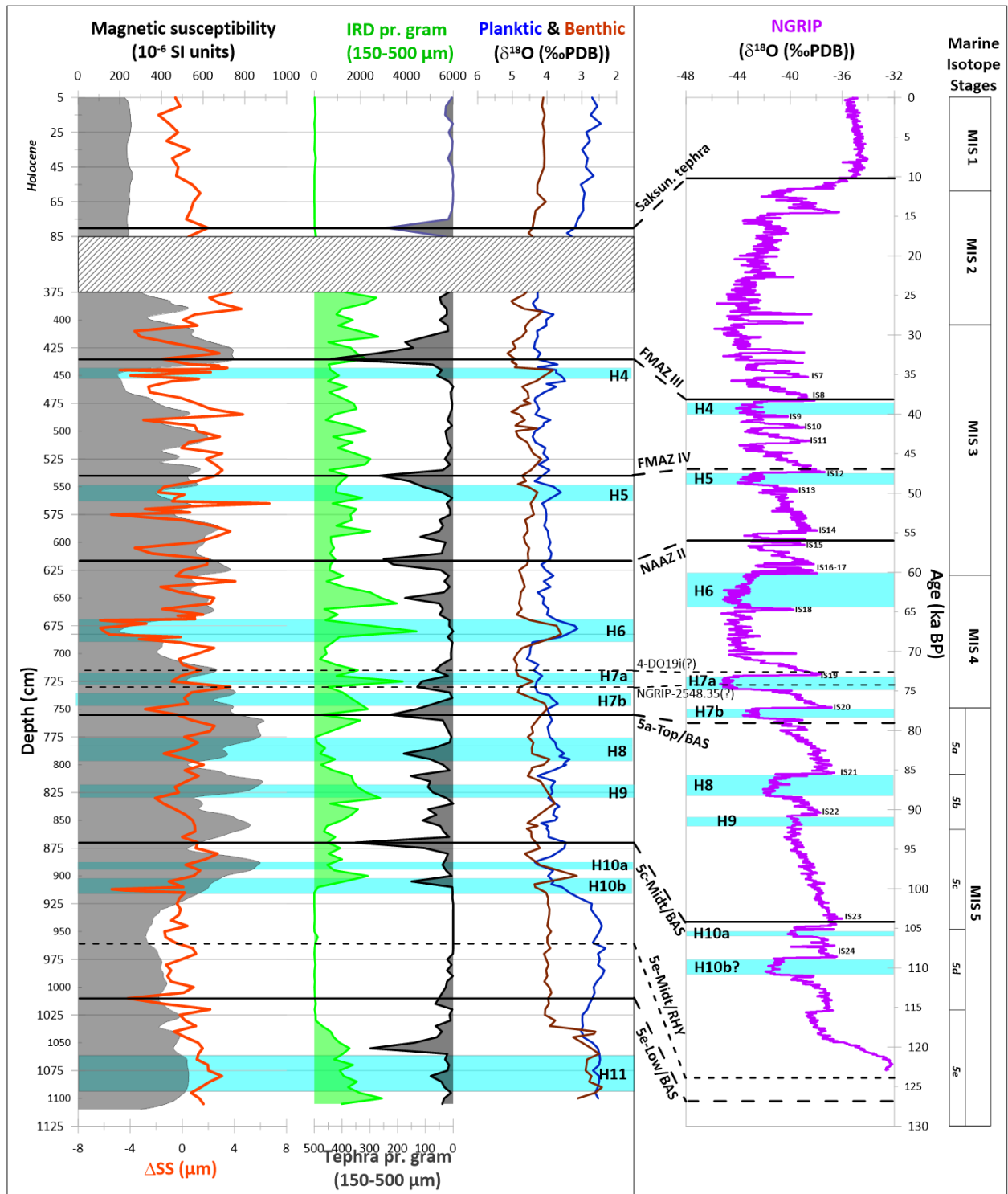


Figure 26: Correlation of the investigated core against the NGRIP. Correlations are done with the ΔSS values (orange). Solid lines are to mark known tephra layers, while dotted lines mark uncertain tephra layers. Heinrich events marked in letters (e.g. H6). The striped box mark the split between the lower part of the core and the Holocene. (Note that tephra at 1005 and 1010 cm have been removed, due to their high tephra content they overshadowed the other layers.)

4.2 Comparison to other studies

Several studies have been done using the sortable silt method since it was approved as a good method to produce paleo bottom currents. Evans, et al. (2007 & 2008) have done several cores testing the Blake Outer Ridge, on the Northeast American continental margin, to document the deep-water circulation in this area. Jessen et al. (2015) focused on the western Svalbard slope. These publications are giving indications of the bottom current strength both south and north of the investigated area, but not on the same depths. Evans & Hall had cores from depths between 2000-5000 meters, while Jessen & Rasmussen had a core tested at 1880 meter depth (Evans & Hall, 2008).

Bianchi & McCave (1999) also documented a thick package of Holocene sediments south of Iceland, and did sortable silt measurements on it.

Evans, et al. (2007) documented \overline{SS} values with a very low mean grain sizes during the 5e and early 5d substages, lower than present-day measurements (in a core at 2590/2595 m water depth). This is explained by a weakened Labrador Sea Water (LSW) production, which would have caused a shoaling or possibly a loss of the upper dynamic limb of the Deep Western Boundary Current (DWBC), which is LSW-sourced at these depths today (Evans, et al., 2007). These results are similar to the results of this thesis, where the mean grain size of MIS 5d-5e results in some of the lowest average \overline{SS} values in the investigated core.

On the other hand, there are major differences during the glacial period. While the results of this thesis show higher \overline{SS} values during interstadials, and lower during stadials, the results from Evans et al. show the higher values during the stadials (Figure 27). Evans explains this with a rapid shoaling of the DWBC and an increased influence of Antarctic Bottom Water (AABW) (Evans, et al., 2007). The mirrored graph compared to the results presented in this thesis, displays a different current regime between the two locations, however the results from Evans and the results of this thesis are pointing towards a reduction of the NADW. Evans, et al. (2007) is also pointing towards a higher average mean grain size after MIS 5e and with bigger changes in the current strength during MIS 4, which is a similar pattern to the investigated core.

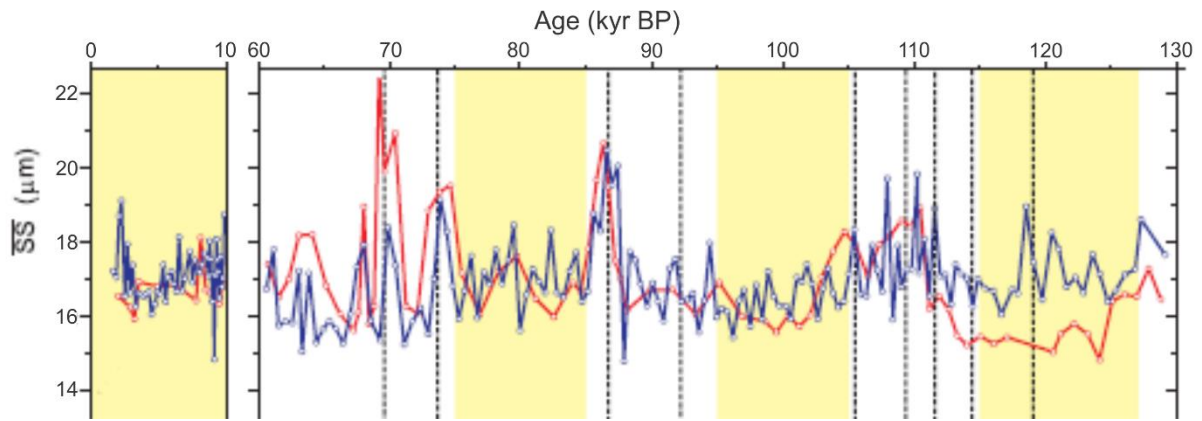


Figure 27: Graph showing sortable silt from cores investigated by Evans et al. (2007). Core 43GGC/1057 (red), at 2590/2595 m water depth. Core 39GGC/1059 (blue) at 2975/2985 m water depth. (Picture modified from Evans et al. (2007).)

Jessen, et al. (2015) did sortable silt analysis on a core from Svalbard. This gives an opportunity to compare sortable silt results from the northern side of the Greenland-Scotland Ridge. The core JM04-025PC was taken from a water depth approximately 700 meters below the investigated core.

The results from Jessen et al. (2015) and the investigated core from the thesis, show similarities in the ΔSS curves. Most changes in current flow correlate, but the investigated core show higher amplitudes. Jessen, et al. (2015) also did measurements with more data-points, giving their core a higher resolution than the investigated core. Variations can also be seen, with H6 lasting shorter in JM04-025PC than in JM11-FI-19PC. Jessen, et al. (2015) also record higher velocities during the cold stadial 19 (Figure 28).

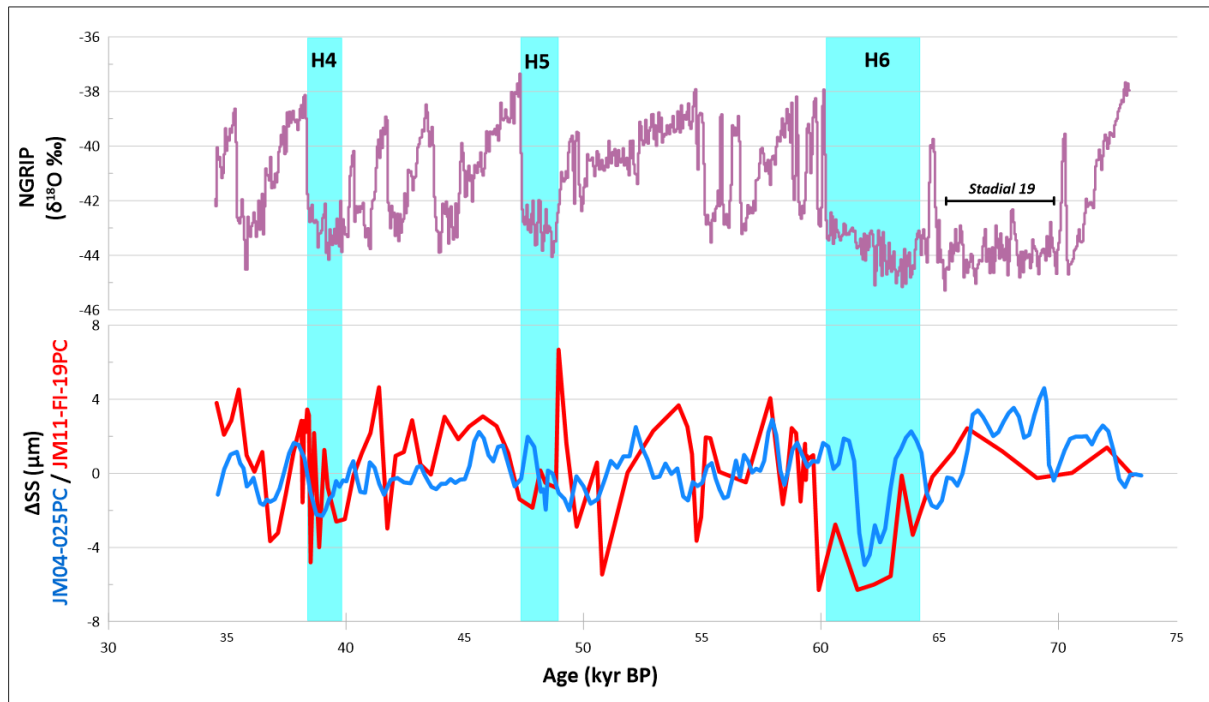


Figure 28: Comparison between the core from Jessen et al. (2015) (Blue), and the investigated core, JM11-FI-19PC (red). Oxygen isotopes from NGRIP in purple and Heinrich events in blue boxes. Stadal 19 marked to the right of H6. (Data for JM04-025PC contributed by Simon P. Jessen)

The differences in ΔSS are probably related to the different depths, and the cores are affected by different current regimes.

The \overline{SS} values from the Holocene is comparable to the investigated core. Even though Jessen, et al. (2015) have more data-points, and a much thicker package of Holocene sediments, the general curve starts high and is decreasing towards present (Figure 29). The average mean grain size is similar, with JM04-025PC averaging 23.8 μm and JM11-FI-19PC averaging 25.5 μm . Higher resolution on the Holocene part in the investigated core, might have led to more similarity with JM04-025PC, however the difference in the amount of sediment also implies less sedimentation or higher current velocities, which would fit the 1.7 higher average in the investigated core.

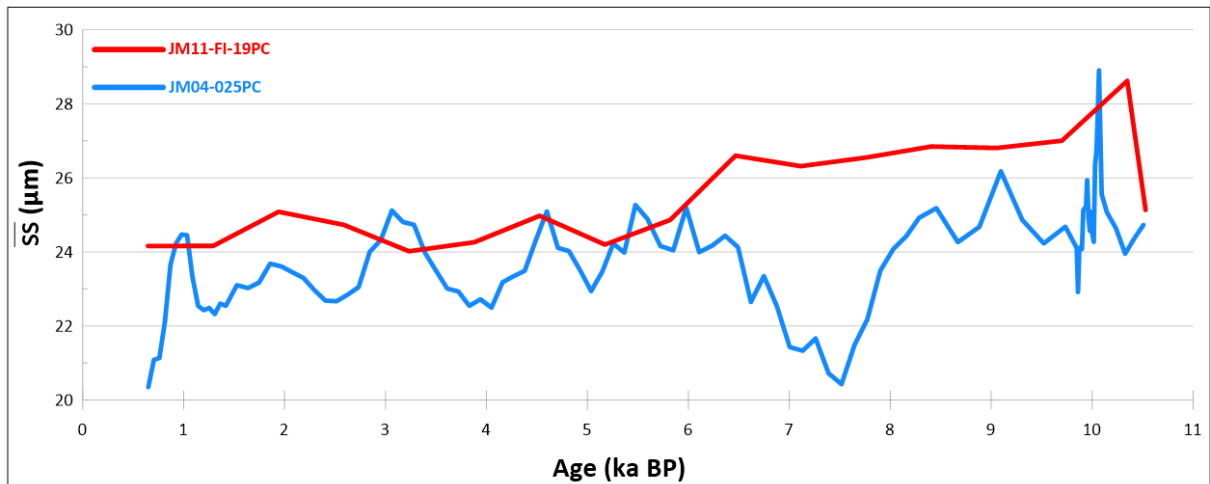


Figure 29: Comparison between the Holocene part of the JM04-025PC from Jessen et al. (2015) (blue), and the investigated core, JM11-FI-19PC (red). Values are given in mean grain size. (Data from JM04-025PC contributed by Simon P. Jessen).

Jessen, et al. (2015) is also mentioning how the mean grain size is higher in the Holocene than during the glacial stage (Jessen & Rasmussen, 2015). This deviates from the investigated core, where the average mean grain size for the glacial stage is higher than both the Holocene and the Eemian interglacials. This will be discussed further down, but this difference might also be caused by the different water depths of the two cores.

Holocene SS-analysis have also been done south of Iceland, where Bianchi & McCave used a core from 2848 meter water depth, containing an almost 450 cm long Holocene record (Bianchi & McCave, 1999). The \overline{SS} results from this core yielded values between 10-16 μm , far below the investigated core. It also showed a lot of fluctuations during the 11.000-year time span, not picked up in the investigated core.

The main reason for the fluctuations not being picked up in the investigated core would be the vast difference in amount of sediments, probably combined with a higher resolution of the \overline{SS} -analysis. The difference in in silt mean average is probably due to the Iceland Basin being more unrestrained than the overflow region of the Faeroe-Shetland Channel, as the overflow water can spread more.

4.3 Deep-water changes

4.3.1 Ice-rafted Silt Biasing

A major input to take into consideration is the ice-rafted silt biasing. The data points showing the highest mean \overline{SS} is also the intervals containing the highest sand content (Figure 7). It is more than likely that the ice-rafted silt has played a role in the high values. However, the $\Delta\overline{SS}$ are showing similar features as the mean \overline{SS} , raising the question about the validity of the sand calibrations over such long time periods. Unit 1 contains the largest differences in sand content and there is a relatively good chance that these differences have affected the sand calibration negatively. One of the reasons for dividing the units as they are done, was to try to limit this error source for the sand calibration. On the other hand, the IRD content and the highest \overline{SS} peaks do not correlate completely. This could again point in the direction that the bottom currents truly were this strong, and that the high sand content at these points are simply a result of the winnowing of finer material. Since the highest peaks of the \overline{SS} have been interpreted to correlate with the interstadials, there should also be less sand deposited, backing up the validity of the high current strength during interstadials.

The $\Delta\overline{SS}$ is showing the changes in current strength (either faster or slower), but it cannot reduce or increase the silt mean grain size to its “true” values. This is why the interpretation of the mean \overline{SS} have been based on the results, and discussed without too much emphasis on the silt biasing. However, it must be pointed out that there are probably a lot of disturbance, especially during MIS 3 in Unit 1

4.3.2 Bottom water current flow during stadials and interstadial

The Faeroe Islands are perfectly located for research of the North Atlantic circulation. It lies in the midst of the northward flowing Atlantic surface water derived from the Gulf Stream system, and the cold Norwegian Sea Overflow Water that flows southwards along the bottom of the Faeroese channels and contributes to the North Atlantic Deep Water (NADW) (Rasmussen, et al., 2002). This part will discuss how the climatic changes during D/O-events affected the bottom current strength and the North Atlantic circulation.

Many sources have found indications of a stop or near stop of the convection in the Nordic

seas during the stadials (e.g. Rasmussen, et al., 2002; Rasmussen, et al., 2004; Rasmussen, et al. (1999); Ezat, et al. (2014); Sarnthein, et al. (1994)). Sarnthein et al. (1994), suggested that the polar front had moved southward, moving the formation of North Atlantic Deep Water (NADW) to south of Iceland (Sarnthein, et al., 1994). Rasmussen, et al. (2004), also found indications for the polar front was moving south of the Faeroe Islands during transitional cooling intervals (Rasmussen & Thomsen, 2004).

Rasmussen, et al. (1996a) proposed that even during the stadials there were some circulation around the Faeroe Islands and the Nordic seas, but consisting of warmer Atlantic water flowing northward beneath a cover of very cold, low saline surface water (Rasmussen, et al., 1996a). Foraminifera assemblages inspected in other sources supports the idea of a warm, intermediate water penetrating into the Nordic seas. Rasmussen, et al. (1996a) found “Atlantic” species in the benthic foraminiferal assemblages during stadials in core ENAM93-21 (Rasmussen, et al., 1996a), while Bassis, et al. (2017) demonstrated through modelling how subsurface warming could trigger the Heinrich-events (Bassis, et al., 2017).

Ezat, et al. (2014) did Mg/Ca-analysis of *M. barleeanus* and *C. neoteretis* to estimate a bottom water temperature (BWT), as mentioned in the result chapter (Ezat, et al., 2014). These results are also a good indicator of the warm, intermediate water. Rasmussen, et al. mentioned that *C. teretis* “is considered to be an indicator of Atlantic Intermediate Water with temperatures above 0°C” (Rasmussen, et al., 1996b), as well as the “Atlantic” species “have not been found in temperatures below 2 °C and most commonly found above 3.5 °C” (Rasmussen & Thomsen, 2004).

As seen in the figure below, all H-events experience bottom water temperatures above 3.5 °C (Figure 30).

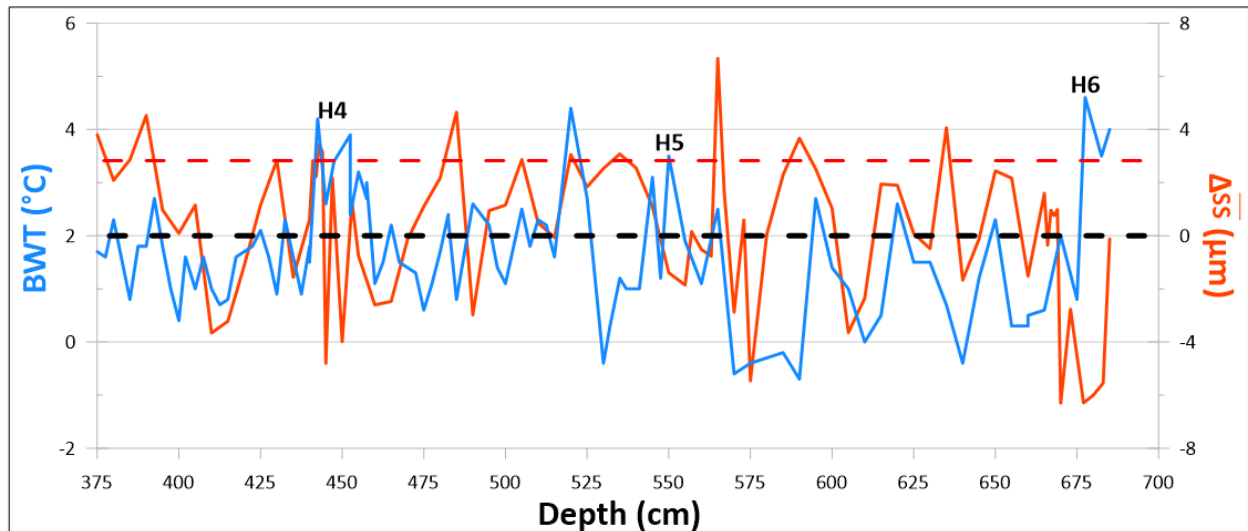


Figure 30: BWT from Ezat, et al. (2014) compared to $\Delta\overline{SS}$ values from JM11-FI-19PC. The dotted black line are dividing the curves at 2°C, and the dotted red line is showing temperatures above 3.5 °C to show where one would expect to find the “Atlantic species” mentioned in Rasmussen, et al. (2004). H-events written in black.

The BWT is showing fluctuations similar to the $\overline{\Delta SS}$, but the general pattern shows that low $\overline{\Delta SS}$ values correlate to higher BWT, and high $\overline{\Delta SS}$ values correlate to lower BWT (Figure 30).

This is consistent with the results found in the \overline{SS} -analysis performed in this thesis. Even though the values of the silt mean size are staggering low during H6 (Figure 7) and generally lower during the stadials than interstadials, there are no indications of a complete stop of bottom water currents around the Faeroe Islands. The \overline{SS} results can only indicate that a current have been present, and not indicate what direction this current had. By using the factors mentioned above it is probable to assume that the current was moving southward, as present-day, during interstadials, and northwards during stadials, but with a weaker current strength (Figure 31).

It is in recent years, agreement about the warm, Atlantic intermediate water in the Nordic seas being an important factor for the rapid changes between stadials and interstadials (e.g. Rasmussen, et al. (2004); Ezat, et al. (2014); Bassis, et al. (2017)). This is contributed to the North Atlantic Drift feeding the Nordic Seas with warmer water, eventually decreasing the density of the water until the halocline gets destabilized and broken (Rasmussen & Thomsen, 2004). The warm, Atlantic water was raised to the surface, getting in contact with the atmosphere, and rapidly heating up the climate. Interstadial conditions, similar to

Holocene, once again restarted the convection in the Nordic seas, and this is showing in the \overline{SS} -results as an increase in bottom current strength.

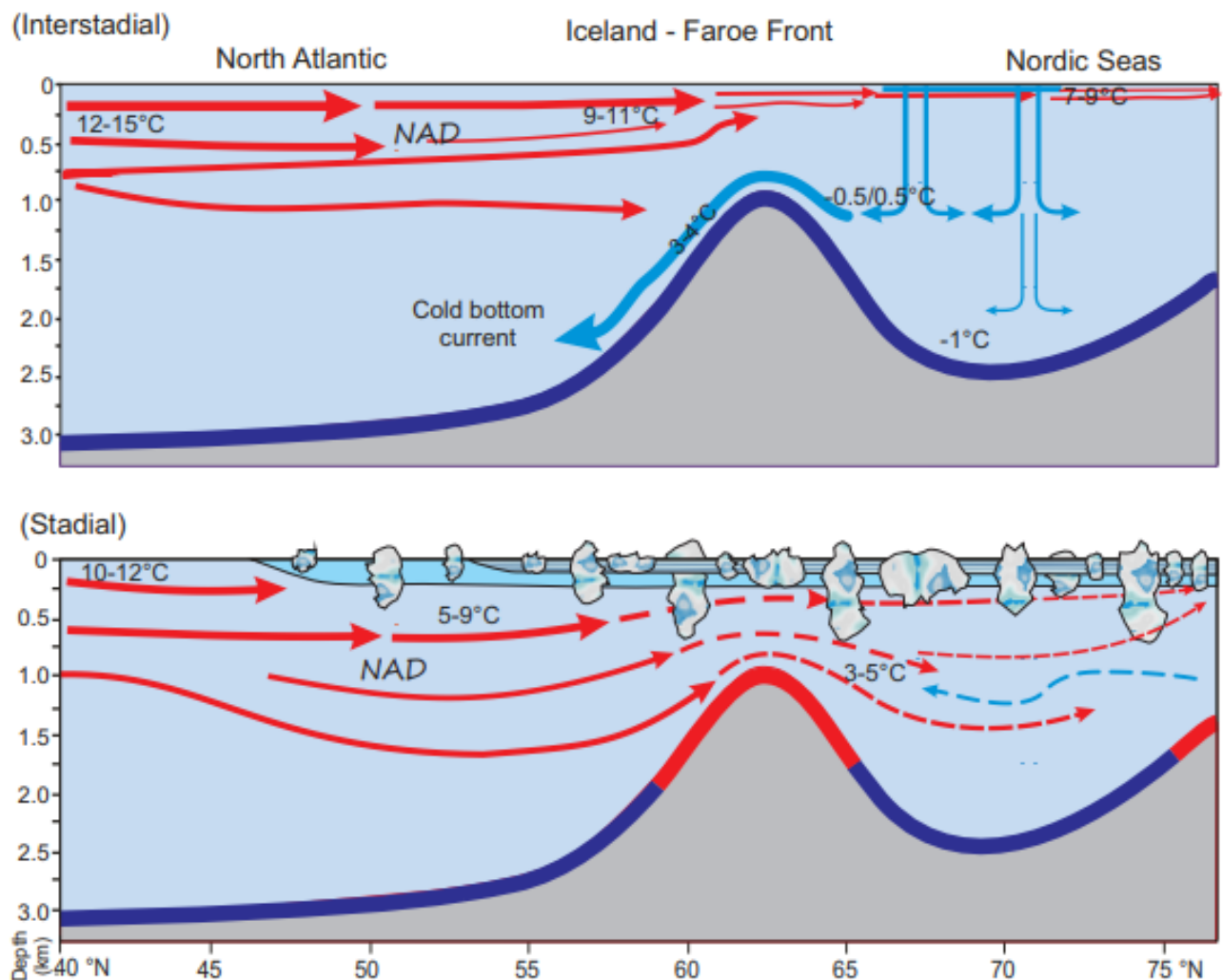


Figure 31: A simplified reconstruction of the possible circulation pattern of the surface- and intermediate-depth water masses during interstadials (above) and stadials (below). Image is a coloured version from Rasmussen, et al. (2004).

One question to ask for further investigations is whether the high stadial \overline{SS} -values were caused by the climatic instability, or if the NAD was feeding the Nordic Seas at such a high pace that it partially caused the climatic instability?

4.3.3 Convection and deep-water changes

The climatic regimes that ruled the Northern Hemisphere was vastly different during the glacial period than it is today. This would also affect the convection regimes during the interstadials. Rudels, et al. (2012) wrote about how convection in the Nordic Seas have changed between 1998 and 2010. In the period of only a decade, he found clear differences in the convection and sea layer regimes (Figure 4) (Rudels, et al., 2012). Considering how the convection regimes can change the layering of the Nordic seas, as Rudels found, the layering might have been affected in a similar condition during the Weichselian ice age. The bottom current changes might have happened because of a thinning or thickening of a layer within the water column. Rudels is mentioning that Atlantic water (AW), Recirculated Atlantic Water (RAW), and Arctic Atlantic water (AAW) could be forced to the center of a gyre and be transformed to Arctic Intermediate Water (AIW), but become restricted within the Greenland Sea, thickening the AIW (Rudels, et al., 2012). It is possible that similar effects could have happened before, where either a thinning or thickening of a layer in the water column could reduce or increase the bottom current strength over the Faeroese Shelf.

The Atlantic Meridional Overturning Circulation (AMOC) is one of Earth's major circulation systems, redistributing heat on our planet and thereby affecting its climate (Caesar, et al., 2018). Caesar, et al. (2018) and Thornalley, et al. (2018) are both arguing for a weakening in the AMOC in their articles. A weakened AMOC would affect the entire circulation system, and thereby affect the currents at the JM11-FI-19PC core. Thornalley, et al. (2018) focused on The Labrador Sea circulation in the duration between AD 1750 to AD 1900 and did \overline{SS} measurements of the deep western boundary current (DWBC). He calculated the estimated speed of the current at two sediment cores at the Black Outer Ridge to be 12 and 14.5 cm/s at AD 1900, compared with 14 and 17 cm/s at AD 1750 respectively (Thornalley, et al., 2018). These current speeds are also closely comparable to the current speeds calculated in this thesis, improving the validity of the velocity calculations, even though there is a difference in water depth. The results Thornalley, et al. (2018) found suggested a decrease in the DWBC of approximately 15% in these 150 years. Caesar, et al. (2018) also concluded with an AMOC decline of 3 ± 1 sverdrups (Sv; $1 \text{ Sv} = 10^6 \text{ m}^3/\text{s}$) since the mid-twentieth century, amounting to 15% as well. Caesar, et al. (2018) argues the changes in the AMOC to the sea

surface temperatures (SST), while Thornalley, et al. (2018) hypothesize that the weakening is due to the Labrador Sea deep-convection.

Thornalley, et al. (2018) is mentioning how density anomalies produced in the Labrador Sea caused by varying deep convection can modify the geostrophic transport and the AMOC strength. As the Labrador Sea is associated with cooling and freshening of the subsurface ocean, a shift to a warmer and saltier subsurface could lead to a state of reduced convection, with only occasional episodes of sustained deep convection (Thornalley, et al., 2018). This can also be supported by Rudels, et al. (2012), who are suggesting that the increase in salinity and temperature of the AIW and the Greenland Sea Deep Water (GSDW) could transform the characteristics in the Nordic Seas (Rudels, et al., 2012).

Variations within the deep convection would certainly affect the \overline{SS} values, and considering that the events above happened during the “stable” Holocene period, one can only assume that the changes in the stadials and interstadial during the Weichselian ice age would have been more vigorous, resulting in bigger amplitudes in the \overline{SS} .

4.3.4 Relative Sea Level

It is shown through the results, and the discussion above, that the high \overline{SS} values indicate interstadial conditions. However, this presents another issue. If Holocene and the Eemian period were to be consider “optimal” periods for convection and deep-water formation in the Nordic seas and the strength of the bottom current (Hass, 2002), one would expect the \overline{SS} values to be at their highest point in these interglacials. This is not the case, with Holocene and Eemian only averaging 24-25 μm , while the interval between MIS 5a to MIS 3 are averaging around 28 μm . Both the highest and lowest points in the graph is located within this interval, but even during the stadials the silt mean size is rarely below 25 μm (with exception of the H-events) (Figure 6). This would indicate that during the Weichselian glacial period the deep-water current regime was different from the interglacial periods (Holocene and Eemian), as mentioned above.

The reason for this difference might be linked to the relative sea level. The relative sea level in the Holocene and Eemian periods were much higher than during the Weichselian ice age (Figure 32). This would push the current regime downwards in the water column during the glacial stage. The most probable cause of the higher current speeds is that a contourite was

passing over the core location during the interstadials. Today, relatively strong bottom water flow occurs over the Faeroe shelf, and contourite deposits are widespread on the Faeroese slopes and in the channels (Nielsen, et al., 2007).

Rasmussen, et al. (1996b) wrote an article based on the core ENAM93-21, located slightly southwest of the JM11-19-PC core, at a water depth of 1020 m. Within the interstadial foraminifera assemblages of core ENAM93-21, Rasmussen, et al. (1996b) found the species *P. bulloides*, which in the Labrador Sea is associated with contourite currents, and today in the Norwegian Sea, *P. bulloides* is most abundant at water depths of about 1000m (Rasmussen, et al., 1996b). *P. bulliodes* was in ENAM93-21 found mainly after the Last Glacial Maximum (LGM), and the distribution of *P. bulliodes* suggesting that the maximum current velocity of the bottom water occurred during the middle Holocene (Rasmussen, et al., 1996a). The suggestion that the maximum current velocity happened before the present-day conditions, could indicate that the contourite was moving upwards in the water column with the increasing relative sea level. If this interpretation is correct, it is plausible to assume that during much lower relative sea levels, this current maximum could have been flowing over, or at least near, the investigated area of this thesis, about 150 meters below the ENAM93-21. The idea of vertical shifts of currents and water masses have also been suggested in multiple publications (e.g. Evans, et al. (2007); Thornalley, et al. (2013); Jessen, et al. (2015)). The presence of a stronger current can also explain the high percentages of sand found at the depths of the highest peaks in the sortable silt (Figure 18). Van Weering, et al. (1998), found a contourite drift marking the middle slope area between 1000 and 1500 m water depth of the NE Faeroe Margin, which would cover the investigated core (van Weering, et al., 1998). However, just as Rasmussen et al (1996b) described the mid-Holocene to be the period of maximum bottom current velocity (Rasmussen, et al., 1996b), one can argue that with the changing relative sea level, the maximum bottom current velocities would change with it. Another clue for this is that the investigated core show the highest current speed at the early Holocene, suggesting that during the interval between the early- and mid-Holocene, the maximum current strength moved from ~1180 m to 1020 m. This would in that case explain the high \overline{SS} values found during interstadials during the Weichselian ice age, where it is plausible that the maximum velocity of the current was continuously moving in the water column.

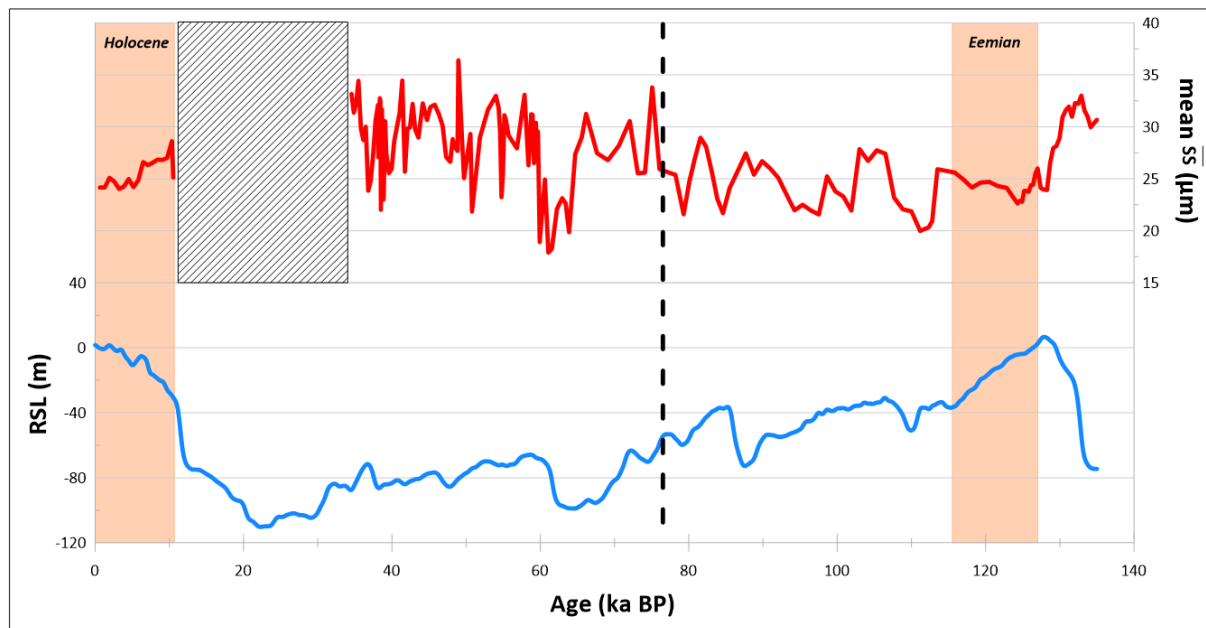


Figure 32: mean \overline{SS} compared to relative sea level (RSL). The dotted line at ~ 78 ka BP is dividing the graph at the point where there is an increase in average mean grain size, and where the RSL is at its lowest. (RSL values from Grant, et al. (2012)).

The figure above shows how the RSL could have played a major role in the mean grain sizes recorded in the core (Figure 32). Between ~ 35 - ~ 78 ka BP (where the graphs are divided), the average mean grain size is $28.5 \mu\text{m}$ and the RSL have an average of -78 m. Above the dividing line, between 78 - 115 ka BP (not including Eemian), the average grain size is $24.3 \mu\text{m}$ and the average RSL at -45 m.

One of the reasons for the connection between the \overline{SS} and the RSL might be due elevation of a water layer above the Greenland-Scotland Ridge. This might affect the water layers close to the bottom, as the RSL might restrict or open the gateway over the Greenland-Scotland Ridge. Basic fluid dynamics tells us that water is incompressible, and the layering of the ocean could thereby be comparable to water passing through a pipe. Depending on the thickening or thinning of the layers, the flow speed of the currents might change (Figure 33).

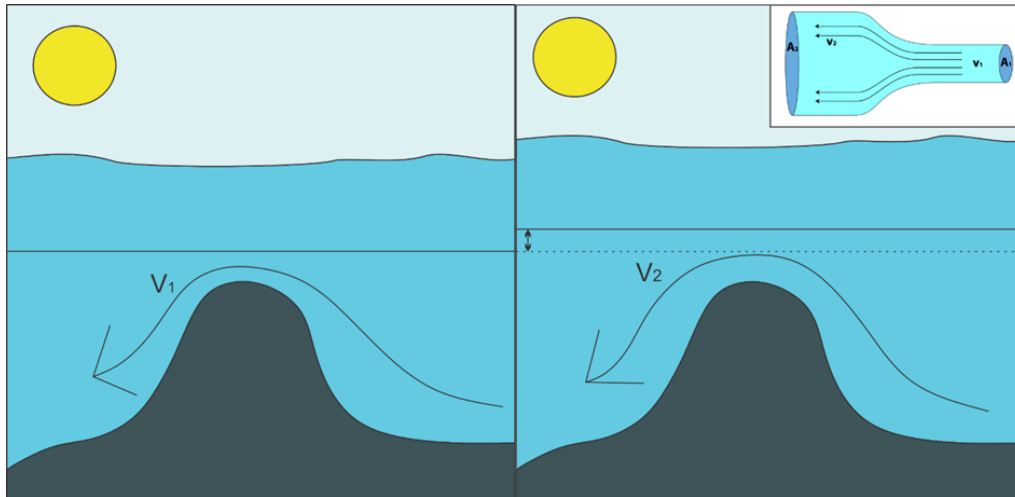


Figure 33: Image showing how sea level rise could affect the deep-water layer going southwards. The expansion above the ridge leads to equal amounts of water being transported, but at a slower pace. In this case: $V_1 > V_2$.

With a larger area to flow through, it would require less velocity to get an equal amount of water through that area, reducing the m^3/s , thereby the Sv , as mentioned above. For now this is just speculation, but considering the relatively high \overline{SS} values recorded during the stadials in MIS 3 and the relatively low values recorded during the Holocene and Eemian, this might be a plausible answer, with NAD entering through a constrained gateway over the Greenland-Scotland Gateway.

If the sea surface velocity of the NAC system during the stadials were comparable to the velocities at present, they would lie well above 10 cm/s around the Faeroe Islands, due to the intensified northeastward flow from the Iceland Basin (Flatau, et al., 2003). From what was discussed earlier, the NAD would flow northwards below a colder and fresher surface layer.

The results found in the estimated bottom current velocities show current speeds of 12-18 cm/s during stadials (Figure 23). It is not certain that the sea surface velocities were as high as present conditions, considering that the flow regime of the sea surface was probably different during stadial conditions with sea ice occasionally covering parts the Nordic seas. Larger parts of the NAD would probably be deflected westwards, or southwards, in the Atlantic as well, due to the density differences of the water masses, but with constriction of the NAD through the Greenland-Scotland Ridge, it might be that the subsurface NAD increases in velocity.

4.3.5 Marine Isotope Stages 3-4

The differences between the \overline{SS} and the RSL seen above (Figure 32) is not only showing that MIS4-MIS3 was an unstable part of the Weichselian ice age, but also that it seems to be building up ice on land. The RSL is generally sinking from the start of Eem, but it is from the start of MIS 4 that the RSL gets really low. The most obvious cause for this would be a build-up of ice on land.

The NGRIP data is showing MIS 3 to be very unstable, with fast fluctuations between the stadials and interstadials. This is also displayed in the \overline{SS} values.

Van Meerbeeck, et al. (2009) noted that the annual precipitation was higher during the MIS 3 stadials than during the LGM, as well as summer temperatures were higher during MIS 3 (van Meerbeeck, et al., 2009). However, it seems that the general climate was cold, as it must have been to reduce the RSL and build up glaciers on land during this period. Xiao, et al. (2015) are using the low or non-existing concentrations of phytoplankton biomarkers to suggest that there must have been perennial and dense sea ice cover from north of the Fram Strait and across the central Arctic Ocean (Xiao, et al., 2015). Cronin, et al. (2012), who use it to explain the deepening of the halocline, also suggests a sea-ice covered Arctic Ocean (Cronin, et al., 2012).

A partly sea-ice covered Nordic Sea with a deep halocline pushing the warm, Atlantic water beneath it is also what seems plausible from the results of the thesis. The $\delta^{13}C$ data from Ezat, et al. (2017), show generally less ventilation of CO_2 during MIS 4 – MIS 2 compared to MIS 5 (Figure 34). The presence of a thick ice cover, or a cold, fresh surface water during parts of the MIS 4 – MIS 3 might have acted as a barrier for the oceanic CO_2 transfer to the atmosphere, before releasing it during the short interstadials (Ezat, et al., 2017).

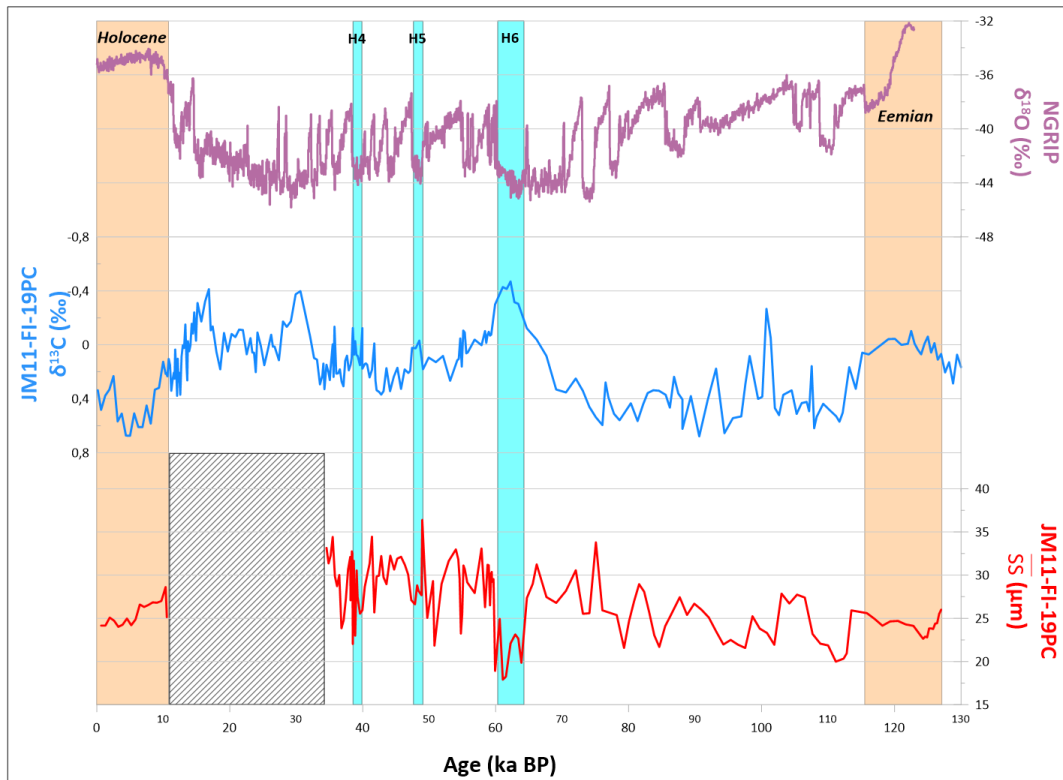


Figure 34: $\delta^{13}\text{C}$ values compared to $\overline{\text{SS}}$ and the NGRIP. Holocene and Eemian interglacials marked in light orange boxes. Heinrich events 4-6 marked with blue boxes.

The climatic fluctuations during MIS 3-4 is apparent in the results of the thesis. The results are pointing towards an instability with a gradual cooling trend (most obvious from the RSL), which culminated in the LGM.

The fluctuations of the IRD counts is another indication for a warm, subsurface water penetrating the Nordic Seas. The smaller, non-Heinrich interstadial warmings might be coupled with the IRD curve fluctuations. These might be engaged by the warm, subsurface water undercutting the marine part of glaciers, melting them from beneath and forcing them to start calving (Bassis, et al., 2017).

4.4 The Holocene and the Eemian interglacials

An interesting comparison is the one between the two interglacials found in the core. The top 85 cm are covering the Holocene period, while the Eemian period is interpreted to lie between 1010 cm and 930 cm. This based on the 5e-Low/BAS tephra layer, and the $\delta^{18}\text{O}$ values recorded by Hoff, et al. (2016). The benthic signal does not change much until at 915 cm in the core, around where H10 has been interpreted, indicating a delayed deep-water signal.

As mentioned above, the Eemian period has a decreasing \overline{SS} value from the start of the interglacial, which flattens out during the middle of the interglacial, then steadily increasing until the end of the interglacial (Figure 35). An interpretation of this could be a reduction in the generation of bottom water. The increased atmospheric temperatures could be a limiting factor for the generation of bottom water, as the waters cool at a slower rate, or had to reach a higher latitude. With a slower cooling period, the density differences between the sea surface and the sinking water would be smaller and would probably flow slower towards the bottom, while a cooling initiated at a higher latitude could mean less production of deep water. Rasmussen, et al. (1999) found evidence that the planktic foraminifera indicated a warmer climate during the Eemian than the Holocene.

This is also consistent with the \overline{SS} results, where the Holocene mean silt size average is slightly above the Eemian average (Figure 35).

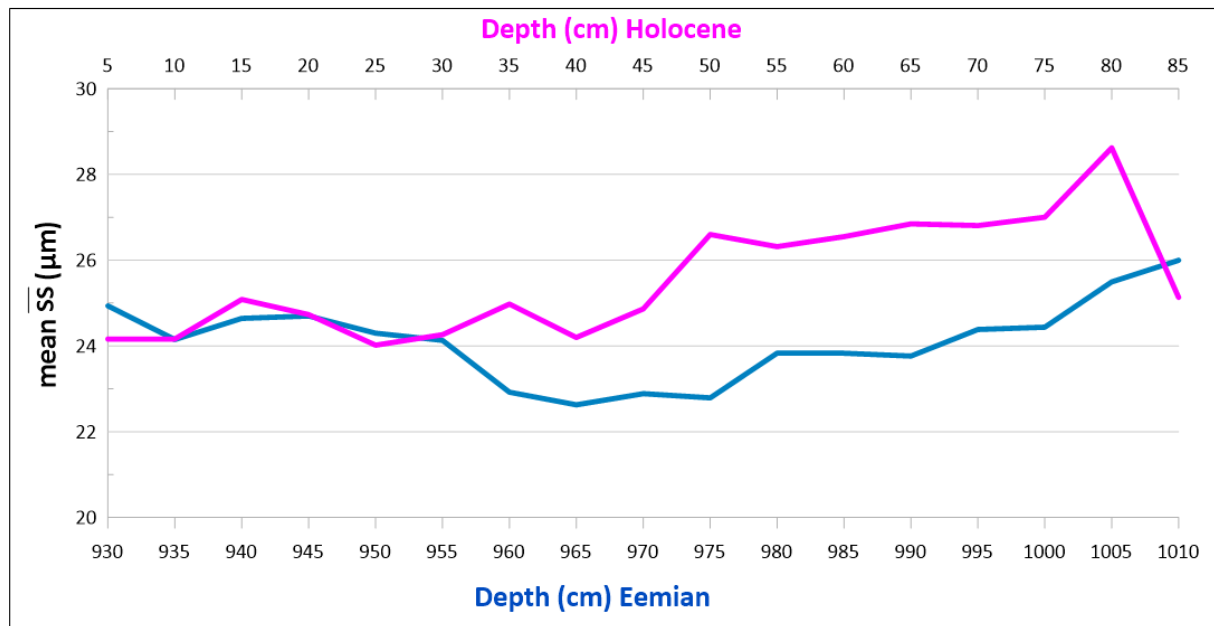


Figure 35: Comparison between Holocene (pink) and Eemian (blue) interglacial.

It is also possible that the contourite mentioned above is weakening downwards in the water column. This would be a fair assumption considering as van Weering, et al. (1998) found that a contourite was moving between 1000m and 1500m water depth. The idea of a decreasing current strength with depth can be argued with the findings of Nielsen, et al. (2007). Holocene sediments are either absent or in very thin patches of sand on the Faeroese shelf, as a result of high current velocities, while there was found high sedimentation rate of fine-grained Holocene material at depths of 1750 m water depth (Nielsen, et al., 2007). The investigated core contains around 12% sand on average in the Holocene part (Figure 21), while the average sand content in the Eemian is around 6% (Figure 20).

As mentioned in chapter 4.3.3, Thornalley, et al. (2018) and Caesar, et al. (2018) investigated a weakening AMOC during the past 150 years, and found it to have weakened by 15% since the mid-twentieth century. Unfortunately, the direct comparison to the investigated core cannot be done, as the youngest part investigated lie at around 600 years of age (about AD 1300-1400, based on average sedimentation per year). However, from the start of the Holocene to that last point (80 – 5 cm) the speed has gradually decreased, from ca. 20 cm/s to 14.5 cm/s, a decrease of almost 30% over roughly 9000 years (Figure 23). This would

imply that the AMOC have been gradually weakening since the end of the Younger Dryas. The velocity decrease from 15 to 5 cm in the core only amount to about 8% (over ~1000-1200 years), so the assumption Thornalley, et al. (2018) and Caesar, et al. (2018) makes about an anomalously weakening of the AMOC during the last 150 years seems valid.

As discussed above, the maximum velocity of the currents are indicating an elevation of the current, suggested to be resulted by rising relative sea level or a thickening of the water layer passing over the investigated core. The enhanced freshwater influxes would be a direct way to apply more water into the oceans, while an increasing SST would lead to thermal expansion. Over the last century, the global mean sea level (GSML) has risen by 10-20 cm, and almost twice as fast the last 20 years (Geographic, 2018).

If the relative sea level is the cause of the weakening AMOC, this might be because of the velocity and pressure around the bottom water currents, as mentioned above.

When now comparing the Holocene \overline{SS} values with the Eemian values, there can be identified a similar trend. From the start of the Eemian, the current velocity is gradually decreasing, just like during the Holocene, before it starts to increase around the mid-Eemian (Figure 35). The increase in bottom current velocity might be linked to the cooling of the climate, as mentioned by Rasmussen, et al. (1999), from around 119 ka BP.

The decline in bottom current strength during the early Eemian period are probably closely linked to what is observed during the Holocene. The AMOC was probably weakening as a result of both the enhanced freshwater influxes and the higher SST. The relative sea level was also higher during the Eemian than at present, which might explain the lower average in \overline{SS} (Grant, et al., 2012). Figure 32 is showing a decrease in the RSL from the start of the Eemian to its end, which might seem similar to the Holocene, but Grant, et al. (2012) is mentioning that due to the uncertainties, the sea-level might have been above 0 m at 126-130 or 120-133 ka BP (in the Red Sea, where he based the research), the latter being very consistent with the increase in \overline{SS} .

The late Eemian cooling from 119 ka BP and the increasing \overline{SS} values might be linked to a breakdown in the AMOC. Because of its role in heat transport, it is assumed that a weakening of the AMOC cools the Northern Hemisphere (Thornalley, et al., 2018). It can be plausible that by the mid-Eemian the AMOC had weakened to a “point of no return”, where

the Northern Hemisphere started cooling and glaciers were once again building up on land. At the end of the Eemian period, the climate in the Northern Hemisphere had declined to such a degree that the NAD once again was pushed below a low-saline halocline, and with less warm water to evaporate, the production of the Nordic Sea overflow halted and the Northern Hemisphere was once again brought into a glacial stage.

Ezat, et al. (2017) is pointing out that there are very different values between the $\delta^{13}\text{C}$ data from the Eemian and the Holocene (Figure 34). This is explained by the higher temperatures during the Eemian than the Holocene which probably caused the air-sea gas exchange to be smaller, resulting in the oceans decreased ability to dissolve CO_2 (Ezat, et al., 2017).

Considering the increasing amount of CO_2 in the atmosphere today and the global rising temperatures (Norby & Luo, 2004), it certainly is a possibility that the rising global temperatures could lead to higher SST, resulting in a smaller amount CO_2 being taken up by the oceans. This could eventually lead to Eemian-like tendencies.

While the Eemian period reached the end of its warm period after around 8000 years (127-119 ka BP), the Holocene still have high temperatures after around 10,000 years. This difference might be caused by the warmer climate during the Eemian. The warmer climate might have led to a faster breakdown of the AMOC, making the Eemian warm period shorter as a result of its high temperatures.

This might be a grim prospect for the Holocene, as we currently are in the midst of a period of global warming (Norby & Luo, 2004). It is possible that the Holocene warm period have lasted this long, precisely because it has not been as warm as the Eemian. However, the estimates are that the global climate will get considerably warmer the next century, or within even shorter time. If one is to expect the two interglacials to follow similar trends, one might believe that the Holocene are reaching its mid-point (Figure 36).

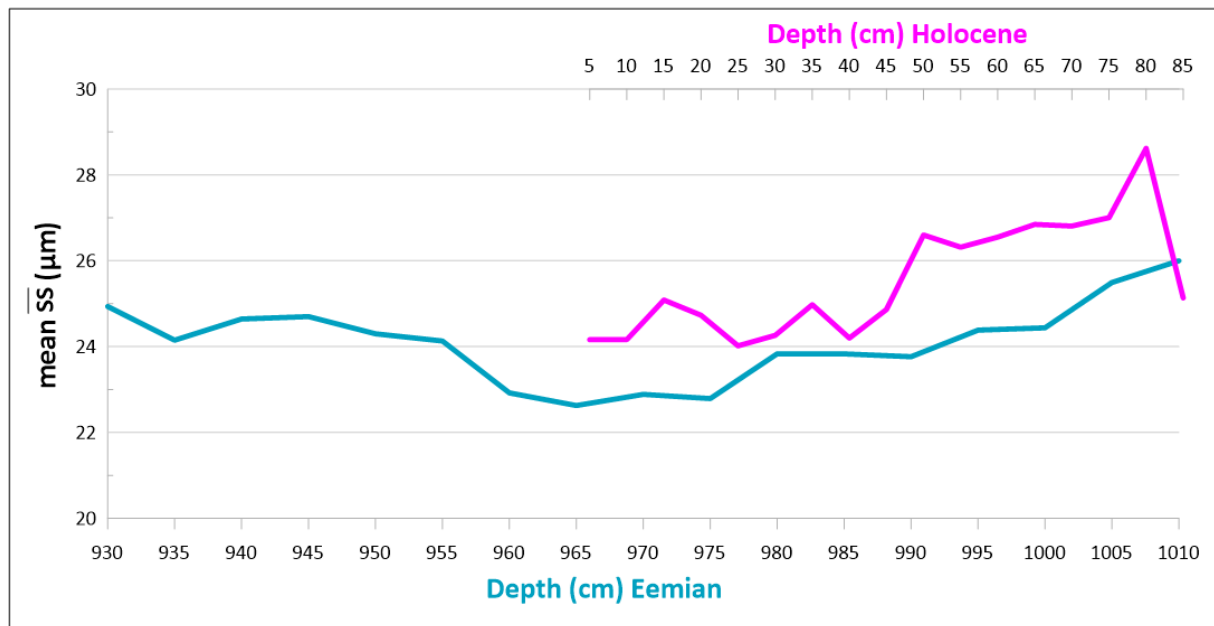


Figure 36: Similarities between the Holocene and Eemian interglacials, assuming that Holocene have not yet reached its mid-point.

If the Eemian is to be viewed as a precursor for what would happen during the Holocene, then this period might also reach a “point of no return” for the AMOC, plunging the Northern Hemisphere back into a transitional cooling leading up to a new glacial period. Moreover, with a relative sea level that have increased substantially over the last 20 years, this might happen faster than expected.

5. Conclusion

The core JM11-FI-19PC have proven itself to be located at an ideal geographical position, as it records how the bottom current strength over the Greenland-Scotland Ridge have been affected by the climatic variations during the last 135,000 years.

Through the thesis it is shown that the method of sortable silt proves valuable for research using deep-sea cores. There are strong indications in the results that supports the idea of higher bottom currents being produced during the interstadials than during stadials. This would give an extra method to use as a correlation for marine cores, when comparing to the Greenland ice cores.

The climatic variations that are recorded in the Greenland ice cores during the last 135,000 years are also recorded in the bottom current strength of the investigated marine core, showing a close correlation between the climate, and the circulation and convection of the oceans.

It is also producing evidence that circulation between the North Atlantic and the Nordic seas never ceased, but shifted directions between the interstadial and stadial phases of the Weichselian ice age. The theory that the production of NSDW must have stopped, or been greatly reduced, during stadials, is also showing through the results and discussion. For the warm, Atlantic water to penetrate down to the core location, it must have been forced down by a strong halocline, without meeting resistance from a colder, bottom water current.

Through the discussion it also seems that this inflow of warm, Atlantic water could have been a triggering mechanism for the Heinrich events, possibly indirectly causing freshwater build-up in the Nordic Seas, which would affect the convection and the AMOC and thereby the bottom current strength.

There also seems to be a strong correlation between RSL and the bottom current strength, but if this could be related to a constriction of an underwater gateway requires further investigations.

The seemingly direct link between the interstadials in the NGRIP and the higher SS values in the core is implying that doing a higher resolution study of the investigated core could lead

to even better correlation between the two, something that would be interesting to examine for further studies.

6. References

- Barker, S. et al., 2015. Icebergs not the trigger for North Atlantic cold events. *Nature*, Volum 520, pp. 333-348.
- Bassis, J. N., Petersen, S. V. & Mac Cathles, L., 2017. Heinrich events triggered by ocean forcing and modulated by isostatic adjustment. *Nature*, Volum 542, pp. 332-335.
- Bassis, J. N., Petersen, S. V. & Mac Cathles, L., 2017. Heinrich events triggered by ocean forcing and modulated by isostatic adjustment. *Nature*, Volum 542, pp. 332-334.
- Bianchi, G. G. & McCave, I. N., 1999. Holocene periodicity in North Atlantic climate and deep-ocean flow south of Iceland. *Nature*, Volum 397, pp. 515-517.
- Bianchi, G., Hall, I., McCave, I. & Joseph, L., 1999. Measurement of the sortable silt current speed proxy using the Sedigraph 5100 and Coulter Multisizer II: precision and accuracy. *Sedimentology* 46.
- Bond, G. et al., 1993. Correlations between climate records from North Atlantic sediments and Greenland ice. *Letters to nature*, Volum 365.
- Bond, G. et al., 1993. Correlations between climate records from the North Atlantic sediments and Greenland ice. *Nature*, Volum 365, pp. 143-148.
- Boudagher-Fadel, M. K., 2015. *Biostratigraphic and geological significance of planktonic foraminifera*. 2nd red. London: UCL Press.
- Bryan, S. P. & Marchitto, T. M., 2008. Mg/Ca-temperature proxy in benthic foraminifera: New calibrations from the Florida Straits and a hypothesis regarding Mg/Li. *Paleoceanography and Paleoclimatology*, 23(2).
- Caesar, I. et al., 2018. Observed fingerprint of a weakening Atlantic Ocean overturning circulation. *Nature*, Volum 556.
- Cronin, T. M. et al., 2012. Deep Arctic Ocean warming during the last glacial cycle. *Nature Geoscience*, Volum 5, pp. 631-634.
- Dansgaard, W. et al., 1982. A new Greenland deep ice core. *Science*, Volum 218, pp. 1273-1277.
- Davies, S. et al., 2014. A North Atlantic tephrostratigraphical framework for 130-60 ka b2k: new tephra discoveries, marine-based correlations, and future challenges. *Quaternary Science Reviews*, Volum 106.
- Elderfield, H. & Ganssen, G., 2000. Past temperature and $\delta^{18}\text{O}$ of surface ocean waters inferred from foraminiferal Mg/Ca ratios. *Nature*, Volum 405, pp. 442-445.
- Evans, H. K. & Hall, I. R., 2008. Deepwater circulation on Blake Outer Ridge (western North Atlantic) during the Holocene, Younger Dryas, and Last Glacial Maximum. *Geochemistry, Geophysics, Geosystems*, 9(3).

- Evans, H. K., Hall, I. R., Bianchi, G. G. & Oppo, D. W., 2007. Intermediate water links to Deep Western Boundary Current variability in the subtropical NW Atlantic during marine isotope stages 5 and 4. *Paleoceanography*, Volum 22.
- Ezat, M. M., Rasmussen, T. L. & Groeneveld, J., 2014. Persistent intermediate water warming during cold stadials in the southeastern Nordic seas during the past 65 k.y.. *Geology*, 42(8), pp. 663-666.
- Ezat, M. M., Rasmussen, T. L. & Groeneveld, J., 2014sup. Supplemental Information for "Persistent intermediate water warming during the cold stadials in the SE Nordic seas during the last 65 kyr".
- Ezat, M. M., Rasmussen, T. L. & Groeneveld, J., 2016a. Reconstruction of hydrographic changes in the southern Norwegian Sea during the past 135 kyr and the impact of different foraminiferal Mg/Ca cleaning protocols. *Geochemistry, Geophysics, Geosystems*.
- Ezat, M. M., Rasmussen, T. L. & Groeneveld, J., 2016b. Supplements for "Reconstruction of hydrographic changes in the southern Norwegian Sea during the past 135 kyr and the impact of the different foraminiferal Mg/Ca cleaning protocols". *Geochemistry, Geophysics, Geosystems*.
- Ezat, M. M. et al., 2017. Episodic release of CO₂ from the high-latitude North Atlantic Ocean during the last 135 kyr. *Nature Communications*, Volum 8.
- Flatau, M. K., Talley, L. & Niiler, P. P., 2003. The North Atlantic Oscillation, Surface Current Velocities, and SST Changes in the Subpolar North Atlantic. *Journal of Climate*, Volum 16, pp. 2355-2369.
- Geographic, N., 2018. *nationalgeographic*. [Internett]
Available at: <https://www.nationalgeographic.com/environment/global-warming/sea-level-rise/>
[Funnet 13 May 2018].
- Gibbard, P. L. & Lewin, J., 2016. Partitioning the Quaternary. *Quaternary Science Reviews*, Volum 151, pp. 127-139.
- Grant, K. M. et al., 2012. Rapid coupling between ice volume and polar temperature over the past 150,000 years. *Nature*, Volum 491.
- Grobe, H., 1987. A Simple Method for the Determination of Ice-Rafted Debris in Sediment Cores. *Polarforschung*, 57(3), pp. 123-126.
- Hass, H. C., 2002. A method to reduce the influence of ice-rafted debris on a grain size record from northern Fram Strait, Arctic Ocean. *Polar Research*.
- Hebbeln, D. & Wefer, G., 1997. Late Quaternary paleoceanography in the Fram Strait. *Paleoceanography*, 12(1), pp. 65-78.
- Heinrich, H., 1988. Origin and Consequences of Cyclic Ice Rafting in the Northeast Atlantic Ocean during the Past 130,000 Years. *Quaternary Research*, Volum 29, pp. 142-152.
- Hoff, U. et al., 2016. Sea ice and millennial-scale climate variability in the Nordic seas 90 kyr ago to present. *Nature Communications*.
- Jessen, S. P. & Rasmussen, T. L., 2015. Sortable silt cycles in Svalbard slope sediments 74-0 ka. *Journal of Quaternary Science*, 30(8), pp. 743-753.

- Johnsen, S. J., 2004. *World Data Center for Palaeoclimatology, Boulder and NOAA Palaeoclimatology Program*. [Internet]
Available at:
<ftp://ftp.ncdc.noaa.gov/pub/data/paleo/icecore/greenland/summit/ngrip/isotopes/ngrip-d18o-50yr.txt>
- Johnsen, S. J. et al., 1992. Irregular glacial interstadials recorded in a new Greenland ice core. *Nature*, Volum 359, pp. 311-313.
- Jouzel, J., 2013. A brief history of ice core science over the last 50 yr. *Climate of the Past*, Volum 9, pp. 2525-2547.
- Kuijpers, A. et al., 1998. Norwegian Sea overflow variability and the NE Atlantic surface hydrography during the past 150,000 years. *Marine Geology*, 152(1-3), pp. 75-99.
- Ledbetter, M. T., 1986. A late pleistocene time-series of bottom-current speed in the Vema Channel. *Palaeogeography, Palaeoclimatology, Palaeoecology* 53.
- MacAyeal, D. R., 1993. Binge/purge oscillations of the Laurentide ice sheet as a cause of the North Atlantic's Heinrich Events. *Paleoceanography*, 8(6), pp. 775-784.
- McCave, I., Manighetti, B. & Robinson, S., 1995b. Sortable silt and fine sediment size/composition slicing: Parameters for palaeocurrent speed and palaeoceanography. *American Geophysical Union*.
- McCave, I., Manighetti, B. & Robinson, S., 1995b. Sortable silt and fine sediment size/composition slicing: Parameters for palaeocurrent speed and palaeoceanography. *American Geophysical Union*.
- McCave, I. N., Manighetti, B. & Beveridge, N. A. S., 1995a. Circulation in the glacial North Atlantic inferred from grain-size measurements. *Letters to Nature*, Volum 374, pp. 149-151.
- McCave, I., Thornalley, D. & Hall, I., 2017. Relation of sortable silt grain-size to deep-sea current speeds: Calibration of the "Mud Current Meter". *Elsevier Ltd.*
- Meincke, J., Rudels, B. & Friedrich, H. J., 1997. The Arctic Ocean - Nordic Seas thermohaline system. *ICES Journal of Marine Science*, Volum 54, pp. 283-299.
- Nielsen, T., Rasmussen, T., Ceramicola, S. & Kuijpers, A., 2007. Quaternary sedimentation, margin architecture and ocean circulation variability around the Faroe Islands, North Atlantic. *Quaternary Science Reviews*.
- Norby, R. J. & Luo, Y., 2004. Evaluating ecosystem responses to a rising atmosphere CO₂ and global warming in a multi-factor world. *New Phytologist*, 162(2), pp. 281-293.
- NorthGRIP community members, 2004. High-resolution record of Northern Hemisphere climate extending into the last interglacial period. *Nature*, Volum 2805.
- Nurnberg, D., Buma, J. & Hemleben, C., 1996. Assessing the reliability of magnesium in foraminiferal calcite as a proxy for water mass temperatures. *Geochimica et Cosmochimica Acta*, 60(5), pp. 803-814.
- Railsback, B. et al., 2015. An optimized scheme of lettered marine isotope substages for the last 1.0 million years, and the climatostratigraphic nature of isotope stages and substages. *Quaternary Science Reviews*, Volum 111, pp. 94-106.

- Rasmussen, T. et al., 2002. The Faroe-Shetland Gateway: Late Quaternary water mass exchange between the Nordic seas and the northeastern Atlantic. *Marine Geology* 188.
- Rasmussen, T. L. et al., 1999. Climate records and changes in deep outflow from the Norwegian Sea ~150-55 ka. *Blackwell Science Ltd.*
- Rasmussen, T. L., Oppo, D. W., Thomsen, E. & Lehman, S. J., 2003. Deep sea records from the southeast Labrador Sea: Ocean circulation changes and ice-rafting events during the last 160,000 years. *Paleoceanography*, 18(1).
- Rasmussen, T. & Thomsen, E., 2004. The role of the North Atlantic Drift in the millennial timescale glacial climate fluctuations. *Paleogeography, Paleoclimatology, Paleoecology*, Volum 210, pp. 101-116.
- Rasmussen, T., Thomsen, E., van Weering, T. & Labeyrie, L., 1996b. Rapid changes in surface and deep water conditions at the Faeroe Margin during the last 58,000 years. *American Geophysical Union*.
- Rasmussen, T., Tomsen, E., Labeyrie, L. & van Weering, T., 1996a. Circulation changes in the Faeroe-Shetland Channel correlating with cold events during the last glacial period (58-10 ka). *Geology*.
- Rasmussen, T. et al., 2003. Stratigraphy and distribution of tephra layers in marine sediment cores from the Faeroe Islands, North Atlantic. *Elsevier B.V.*
- Robinson, S. G., Maslin, M. A. & McCave, N. I., 1995. Magnetic susceptibility variations in Upper Pleistocene deep-sea sediments of the NE Atlantic: Implications for ice rafting and paleocirculation at the last glacial maximum. *Paleoceanography*, 10(2), pp. 221-250.
- Rudels, B. et al., 2012. The East Greenland Current and its impacts on the Nordic Seas: observed trends in the past decade. *ICES Journal of Marine Science*, 69(5), pp. 841-851.
- Sarnthein, M. et al., 1994. Changes in the east Atlantic deepwater circulation over the last 30.000 years: Eight time slice reconstructions. *Paleoceanography*, 9(2).
- Shackleton, N. J., 1969. The last interglacial in the marine and terrestrial records. *The Royal Society*, Volum 174, pp. 135-154.
- Thornalley, D. J. et al., 2018. Anomalously weak Labrador Sea convection and Atlantic overturning during the past 150 years. *Nature*, Volum 556.
- van Meerbeeck, C. J., Renssen, H. & Roche, D. M., 2009. How did Marine Isotope Stage 3 and the Last Glacial Maximum climates differ? - Perspectives from equilibrium simulations. *Climate of the Past*, Volum 5, pp. 33-51.
- van Weering, T. et al., 1998. Sediments and sedimentation at the NE Faeroe continental margin; contourites and large-scale sliding. *Marine Geology*, Volum 152.
- Wastegård, S. & Rasmussen, T., 2001. New tephra horizons from Oxygen Isotope Stage 5 in the North Atlantic: correlation potential for terrestrial, marine and ice-core archives. *Elsevier Science Ltd.*
- Wastegård, S. & Rasmussen, T., 2014. Faroe Marine Ash Zone IV: a new MIS 3 ash zone on the Faroe Islands margin. *Marine Tephrochronology*.

WHOI, 2018. *Woods Hole Oceanographic Institution*. [Internet]
Available at: <http://www.whoi.edu/page.do?pid=8415&tid=7342&cid=8087>

Xiao, X., Stein, R. & Fahl, K., 2015. MIS 3 to MIS 1 temporal and LGM spatial variability in Arctic Ocean sea ice cover: Reconstruction from biomarkers. *Paleoceanography*, Volum 30, pp. 969-983.